Article

JVC

Journal of Vibration and Control
18(14) 2210–2233

DOI: 10.1177/1077546311429339
jvc.sagepub.com
SAGE

An experimental comparative study on non-conventional surface and interface damping techniques for automotive panel structures

Yi Liu, Markus Zogg and Paolo Ermanni

Abstract

In order to increase the comfort of vehicle drivers, automotive panel structures are normally damped on their surfaces. Common surface damping treatments like free layer damping or constrained layer damping have the drawback of heavy weight and temperature as well as frequency dependent damping performance. New alternatives with simple structure, high robustness and light weight are sought. In this contribution, three different passive and active damping approaches were investigated: interface damping (ID), active constrained layer damping (ACLD) and particle damping (PD). They were surveyed under same boundary conditions and their performances were compared in terms of weight. The results show that ID strongly decouples the vibration from the source to the panel and provides steady performance over the whole frequency range. ACLD is a lightweight treatment with high damping capability for special mode shapes. PD is an effective simple damper providing excellent damping performance.

Keywords

Active constrained layer damping, automotive panel, comparative study, interface damping, particle damping, vibration measurement

Received: 1 June 2011; accepted: 1 October 2011

1. Introduction

Panel structures in automotive bodies are prone to vibration due to various vibration sources such as engines, trains or wind. Therefore the panels are usually treated with damping systems. Commonly, two surface treatments are applied: free layer damping (FLD) and constrained layer damping (CLD) (Johnson, 1995; Jones, 2001). In free layer damping the panel is covered with one layer viscoelastic material (VEM). With the bending deformation on the panel during vibration, this VEM layer is also bended. Attributable to the extensional/compressional stress in the VEM layer, energy is dissipated. In constrained layer damping, one additional layer (typically metallic), which has a much higher stiffness than the VEM layer, is glued onto the VEM layer. In this case, the bending deformation of the plate induces dominantly shear stresses in the VEM layer. The performance of the CLD is enhanced significantly compared to FLD. These two approaches provide remarkable damping, whereas the properties of the VEM are strongly dependent on temperature and frequency. The application should be designed carefully respecting these two aspects. Furthermore, the weight of VEM is another aspect which should be reduced or improved. New approaches with high damping-weight performance and reliability under harsh environment are sought in order to overcome the drawbacks of FLD and CLD, and to improve the comfort of passengers.

This paper presents alternative damping approaches with regard to their potential to substitute the classical VEM dampers. According to the results in the previous

Centre of Structure Technologies, ETH Zurich, Zurich, Switzerland

Corresponding author:
Yi Lu, Centre of Structure Technologies, ETH Zurich, Leonhardstrasse 27, 8092, Zurich, Switzerland
Email: liuyi@ethz.ch

project phase (Liu et al., 2010), three approaches with good performance on beam specimens were chosen: interface damping (ID), active constrained layer damping (ACLD) and particle damping (PD). Since the vibration behavior of plates (3D bending and torsion) are different and more complex than beams (2D bending), the validation of the damping performance on plate is necessary. Also the previous tests using the phase shift principle could only be exerted under low frequencies. For the system dynamic behavior, a wider frequency range should be investigated. Thus, the three approaches were surveyed on panel structures in this contribution using a free hanging test, which evaluates damping at resonances in a large frequency range.

In Section 2, these damping approaches will be introduced. The measured parameters and process algorithms will be explained. The experimental setup and specimen configurations are introduced in Section 3. Section 4 gives the results of each specimen and some comparisons in detail for each approach. In section 5, the performances of the different dampers are compared transversely. And a conclusion for their applicability will be given.

2. Theory of damping and characterization

2.1. Damping approaches

Interface damping (ID) employs damping material at the interface of the panel and its peripheral structures. In comparison to most well known surface treatments, the concrete effect and performance of the dampers located at the interface of the panel structures have not been systematically studied. According to authors' results (Liu et al., 2010), ID with a small amount of applied VEM has a similar weight specific efficiency as the PD. The traditional surface dampers are normally located sectionally on the surface. If the location of the damper is on a node or a position close to nodes, the vibrations are not suppressed or are weakly suppressed at certain modes. Unlike normal surface treatments, if the plate is treated by ID, the VEM at the interface provides steady damping for every mode at different frequencies. Concurrently, the vibration from the source is partially isolated to the panel through the interface damper, which has a much lower stiffness than the two main joint structures.

Active constrained layer damper is a damping treatment using piezoelectric elements and viscoelastic materials. On the surface of the panel, a piezo sheet sensor is glued to detect the deformation of the panel. One VEM layer is bonded on top of this sensor. An additional piezo sheet incorporating actuation is capped on the viscoelastic layer. All these three layers are collocated across the thickness direction. The voltage signal from the sensor is amplified and inversely fed back to the actuator during the vibration. This leads to an enhancement of the shear stress in the VEM layer caused by the interaction of the piezo actuator and improves the dissipation of energy in VEM. Additionally, the actuator provides an active counter force/moment against the vibration of the primary structure (Stanway et al., 2003).

The particle damper (PD) is an approach which has been investigated for a few decades. Originally a single slug was used to exchange impact energy and momentum between itself and the vibratory structure (Masri, 1970; Bapat and Sankar, 1985). Its performance was further developed by substituting the slug with numerous particles so that the collision time between the primary structure and the damper will be prolonged. As a consequence, the possibilities of energy transfer, friction and dissipation are heightened (Popplewell and Semercigil, 1989; Panossian, 1992).

2.2. Damping characterization

Sine-sweep test is a traditional method to predict the modal parameters of a structure. In our investigation, we implemented the modal testing in a freely supported condition (free-free), because it is notoriously difficult to establish other support conditions appropriately in practice (Ewins, 2000). As a result, the frequency response functions (FRF) were attained. The damping of the plate is evaluated with the magnitudes of the FRF, which is calculated at each measured frequency with:

$$\mathrm{FRF}_{\mathrm{Receptance}} = 20 \cdot \log\left(\left|\frac{\mathrm{x}}{\mathrm{F}}\right|\right) \tag{1}$$

$$\mathrm{FRF}_{\mathrm{Mobility}} = 20 \cdot \log\left(\left|\frac{\mathrm{v}}{\mathrm{F}}\right|\right) \tag{2}$$

x is the response displacement of the structure, v the velocity of the structure and F the input force of the excitation. The receptance FRF reflects information about the system response of deformation and decays rapidly with the increase of frequency. Normally the mobility is used for the FRF evaluation instead of receptance because it decays slower than receptance. In this paper, the mobility was also evaluated.

Since the behavior of the whole plate should be determined, a mean transfer mobility was calculated, which is the root mean square (RMS) value of all measured points on the plate:

$$\mathrm{FRF}_{\mathrm{Mobility,\ plate}} = 20 \cdot \log\left(\sqrt{\frac{\sum_{i=1}^{m}\left|\frac{v}{F}\right|^2}{m}}\right) \tag{3}$$

where m refers to the number of the measured points.

With the magnitudes of the FRF, the modal loss factor of the system is calculated. The loss factor of each mode is assessed with the fraction power bandwidth method (ASTM-E756, 2005).

$$\eta = \frac{1}{\sqrt{(10)^{\frac{n}{10}} - 1}} \cdot \frac{\Delta\omega}{\omega_{res}} \tag{4}$$

Where n denotes the n dB amplitude decay in frequency domain, $\Delta\omega$ is the frequency range of the n dB decay and ω_{res} is the resonance frequency of the system. According to (ASTM-E756, 2005), the value of n should be chosen between 0.5 and 3 dB in the experiments.

2.3. Data evaluation

The aforementioned theory of evaluating the loss factor based on the definition of a single-degree-of-freedom (SDOF) system. Tracing back to the theory, the correct loss factor should be calculated only with a SDOF-shape preserving resonance curve, which is normally not obeyed with the mean FRF curve acquired from equation (3). Therefore, additional measures are entailed to fit the realistic FRF curve into a SDOF system curve for the assessment of modal damping. An optimization tool was developed for this purpose. The modal magnitude of an SDOF system is:

$$\mathrm{r} = \frac{\omega}{\omega_{\mathrm{res}}} \tag{5}$$

$$\mathrm{A}_{\,\mathrm{Resonance}} = 20 \cdot \log\left(\frac{\mathrm{A}'}{\sqrt{(1-\mathrm{r}^2)^2 + (2\zeta \mathrm{r})^2}}\right) \tag{6}$$

Where ω denotes the varying frequency, r is the frequency ratio between the varying and resonance frequency, A' is the amplification ratio of the mode and ζ is the damping ratio.

The RMS curve of the whole plate will be fitted according to equations (5) and (6). By using the least square optimization algorithm of Levenberg-Marquadt (Levenberg, 1944; Marquardt, 1963), the modal parameter ω_{res}, A' and ζ will be determined in the equations. The fitted curve with the addressed parameters ω_{res}, A' and ζ will be further interpolated as shown in Figure 1. The accurate resonance frequency, amplitude and loss factor will be evaluated with this interpolated curve. Actually the loss factor and the resonance frequency can already be acquired with the fitted parameter in equations (5) and (6) without data interpolation. Their values do not change noticeably after the interpolation by using fraction power bandwidth method. Only the exact amplitude of the resonance must be acquired through the interpolation.

3. Experimental

3.1. Experimental setup

The experimental setup is illustrated in Figure 2. The specimen is hung with two elastic wires which are fastened in a stiff and massive test rig. The shaker is connected with an impedance head and further fixed to the frame of the sample (see Section 3.2). A sine-sweep signal is generated, amplified and sent to the shaker as the excitation signal. The input force on the frame and the response displacement on the specimen will be acquired with the impedance head and a laser, respectively. The signal of force is further amplified to a voltage signal additionally through a charge amplifier. The amplified force and measured displacement signals are filtered with a low pass and processed in Labview®. Independent from the main measuring chain, another amplification loop was needed for the ACLD treatment by using two amplification stages (see Section 4.3).

3.2. Plate sample arrangement

The whole undamped specimen is made of aluminum and consists of two components: the frame and the plate. The frame is a sandwich structure with an aluminum honeycomb core and two aluminum facings. The frame has a rectangular hole in the middle. The plate is glued to the surface on one facing. Both parts are centrically collocated. The dimensions can be seen in Table 1. Further parameters of the applied dampers will be presented in chapter 4 with their particular configurations.

Mostly, the vibration of panels in an automotive is induced by the vibration from its peripheral structures (structure-borne noise). The aim of using the sandwich frame is to yield a realistic environment for this kind of vibration transmission. Thus, the sample was excited on the frame and the response was measured on the plate. For the ACLD and PD samples, the plate is glued to the frame with a rigid epoxy, while instead VEM is used for the ID sample at the interface of plate and frame.

Furthermore, we would like to transmit most of the vibration into the plate and have little influence from the frame. For determining the mode patterns of the whole specimen, a modal analysis was done in Ansys® under free-free condition as in the experiments. According to the results, there are 10 modes in total existing up to 400 Hz as indicated in Figure 4 (only the nodes on the plate were extracted in the figure). Then a harmonic analysis with the same boundary

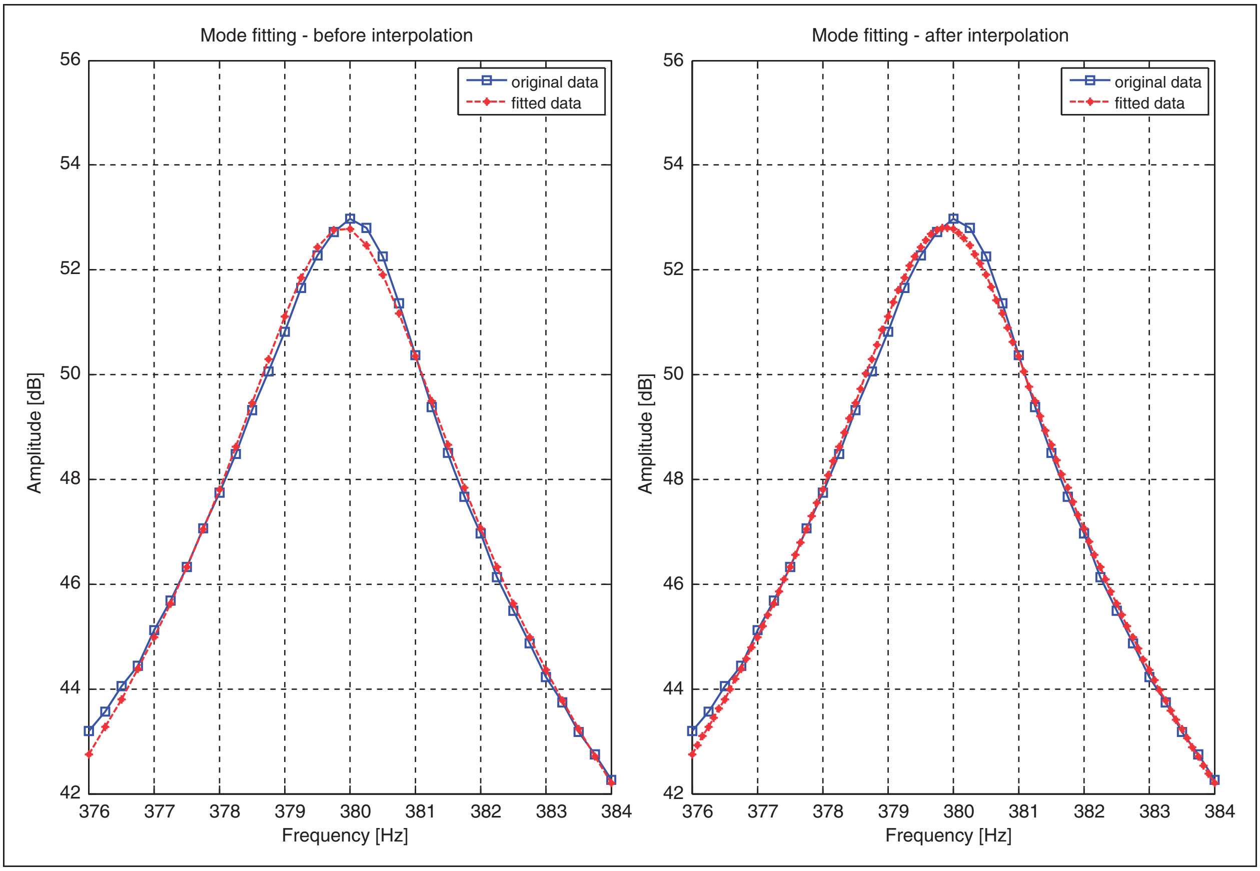

Figure 1. Curve fitting for the evaluation of the loss factors.

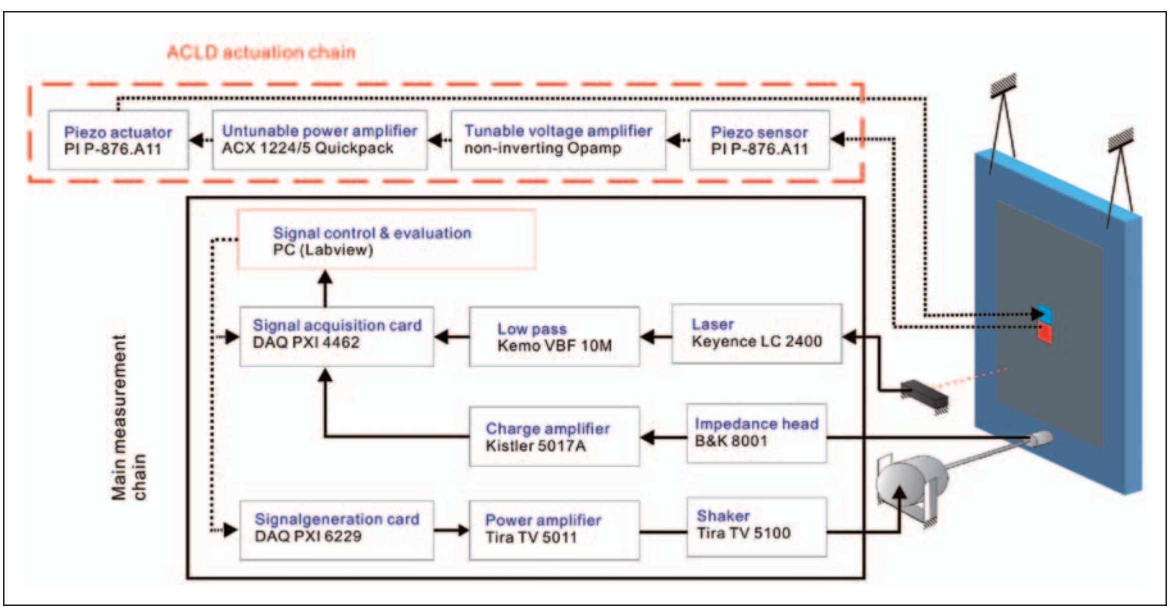

Figure 2. Measurement chain of the experiment.

conditions was performed discretely at these 10 eigenfrequencies to acquire the exact amplitudes of these modes. As shown in Figure 4, the immense stiffness difference between the sandwich frame and the monolithic plate guarantees that the frame possesses only one eigenfrequency (mode 6) up to 400 Hz, whilst the plate already has other nine modes in this frequency range.

3.3. Optimization of damper comparability and size

In order to compare the damping approaches ACLD and PD under similar conditions, the size of the sectional dampers are chosen with similar values: The applied commercial piezo-patch has a sectional size of 61×35 mm. It results in the size of the ACLD damper having the same sectional area. Therefore, the PD's area is chosen with a close value of 60×30 mm. The typical edge width of the bonded area on a vehicle panel is about 20 mm. The area of ID is thus chosen with this value.

Another important aspect for the comparison of the different approaches is to consider the position of the dampers. For ID, no sophisticated positioning is required. The damper will be simply applied homogeneously at the whole interface edges. For the surface treatments, panels are typically treated with local surface dampers which do not cover the whole surface. The localization of the surface dampers is an important issue. In order to find the optimal damper location, the vibration behavior of an undamped plate was at first investigated. The amplitudes of all modes up to 400 Hz were accumulated into one plot. From this plot it can be seen on which position the plate has the highest amplitude through the whole frequency range. In order to get the comprehensive behavior of the plate, both receptance and mobility were accumulated. Figure 5 shows the overlapped receptance and mobility. The entirely accumulated amplitudes from mode 1 to 10 on the left side distributes in the same pattern as the first mode, which reveals that the first mode is apparently dominant among all the modes. In order to take other modes also into account, the amplitudes were additionally accumulated apart from the first mode on the right side of the diagram. We can observe that the middle region of the plate still has the highest mobility. The receptance also reaches 80% of the highest value at this place. Thus, the midpoint is the best position for PD. Since ACLD should be arranged by the modal strain energy approach (Ro and Baz, 2002) instead of the vibration amplitude, the strain energy on the plate of the modes up to 400 Hz was also accumulated like the process mentioned above. In Figure 6 it can be seen

Table 1. Geometry of the sample

Outer dimension of the frame	600 mm × 480 mm
Inner dimension of the frame	400 mm × 300 mm
Thickness of honeycomb core	40 mm
Honeycomb cell size	Ø6
Honeycomb density	54-80 kg/m^3
Face thickness of the frame	2 mm
Panel dimension	440 mm × 340 mm × 1 mm

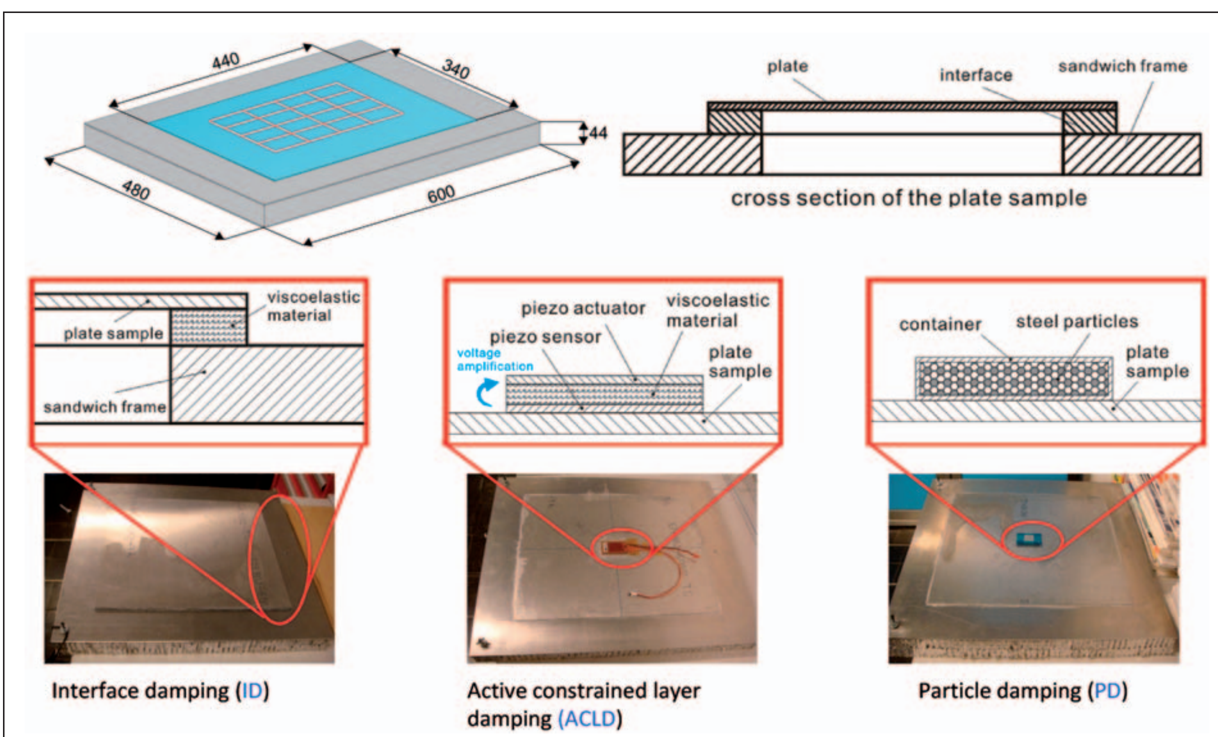

Figure 3. Sample size and configurations.

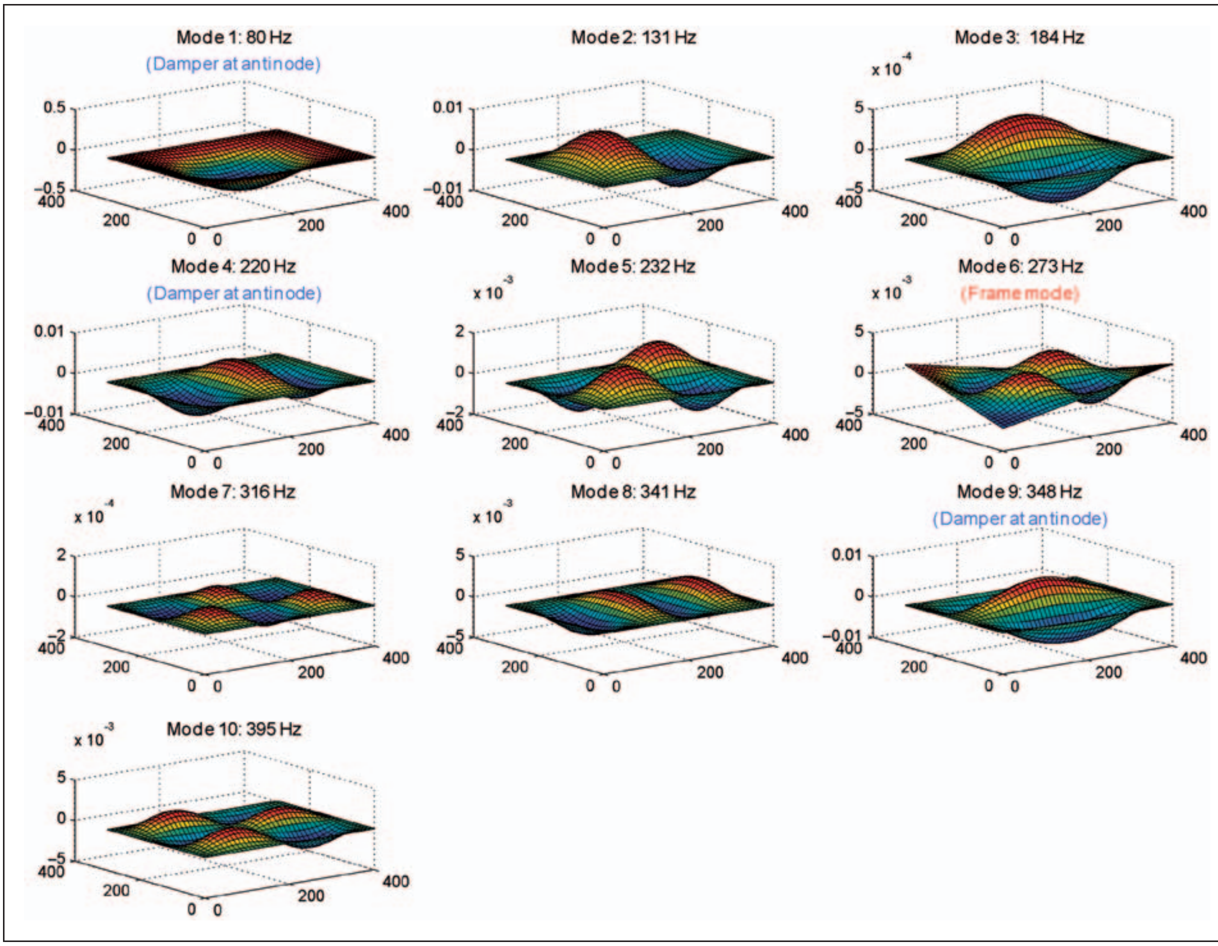

Figure 4. Eigenfrequencies of the plate in the simulation.

that the maximal strain energy of all modes is actually concentrated in a narrow region at the longitudinal edges of the plate, whereas the midpoint has only about 70% of the maximal strain energy. Apart from mode 1, the midpoint becomes the most dominant position. Considering the dimension of the piezo patch, dominance at all other modes and the comparison with PD, the midpoint is a good choice for the placement, although it may hamper the effectiveness of ACLD at mode 1.

With regard to all these aspects, we decided to place the sectional dampers (ACLD and PD) in the middle of the plate covering an area of ca. 60×30 mm. As indicated in Figure 4, the midpoint of the plate is antinode at mode 1, 4 and 9. For these modes, the damper performs significantly due to the great plate displacement/velocity. Thus, by using this "direct" method and placing the damper at the midpoint, the 10 modes of the plate can be divided into three types:

- Damped modes: mode 1, 4 and 9 with antinodes at the midpoint. These modes are supposed to be greatly damped with sectional damper in the middle (ACLD and PD)
- Undamped modes: mode 2, 3, 5, 7, 8 and 10 with nodes at the midpoint. These modes are supposed to have no damping with sectional damper in the middle (ACLD and PD)
- Global modes: mode 6 sourcing from the eigenmode (torsion) of the frame

It should be mentioned that this "direct" method considers the most dominant modes in the structure. However, it loses the controllability at modes with the node position at the midpoint of the plate. Furthermore, other modes with insignificant amplitudes will hardly be concerned. If global optimization is needed, the methodology based on controllability gramian (Hac and Liu, 1993) can be applied. This algorithm takes the places with the greatest mean nodal energies at all modes for monitoring and suppressing the vibration. The difference between the two algorithms is that with the determined position of the direct method, the three mentioned modes can be damped with maximized

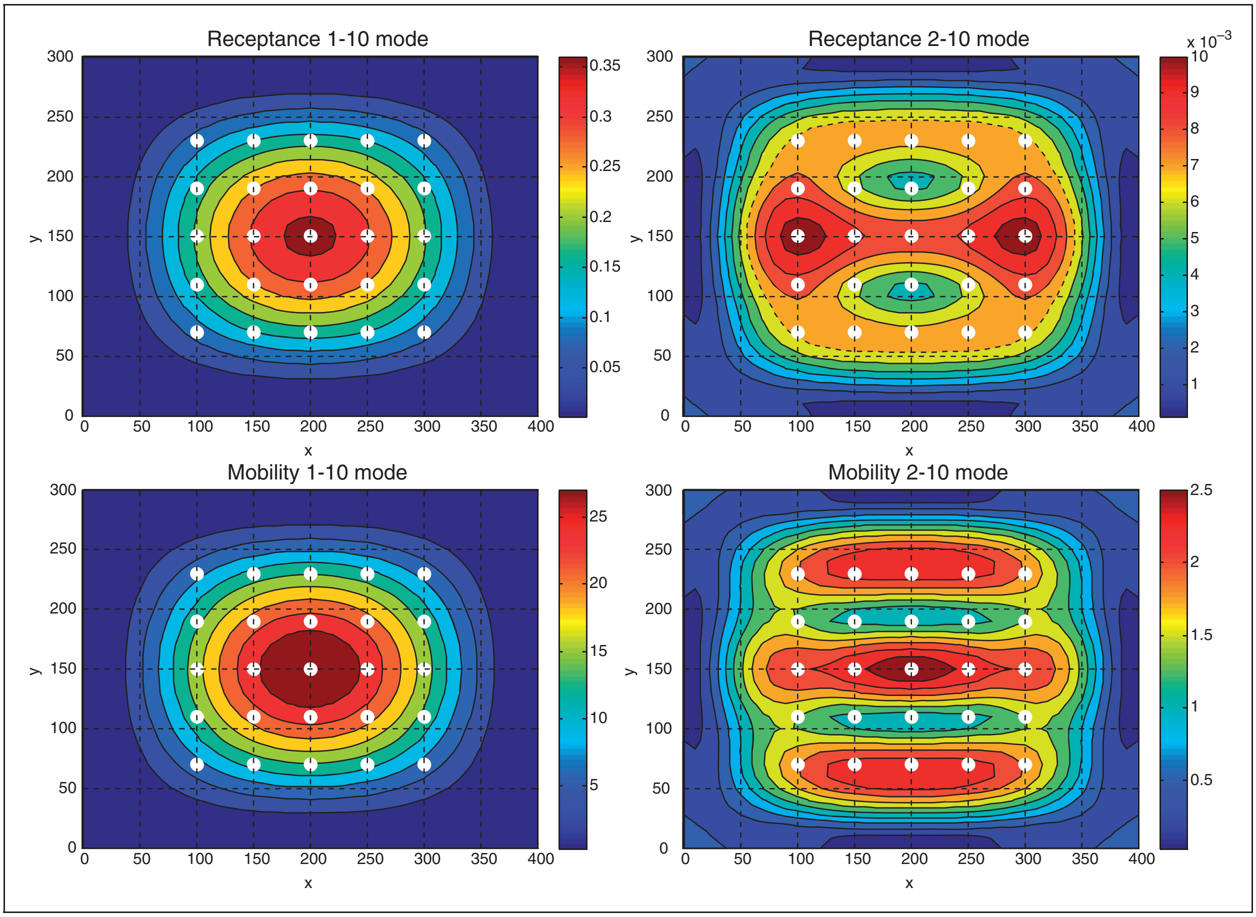

Figure 5. Overlapped amplitudes of receptance and mobility.

damper performances, because the damper is directly located at the anti-node. The difference of loss factors between the damped and undamped modes becomes distinct. If the method based on gramian is used, although every mode will be damped, the compromise between sacrificing and balancing performances among different modes will be undertaken. The difference between modes will be reduced. For a sectional damper contributing little damping, it is hard to distinguish its own damping efficiency from the slight inherent damping from the measurement setup. To make sure that all three investigated damping approaches could be measured with significant loss factors and be compared with their best performances, the direct method was therefore used in this paper.

3.4. Test condition

The specimen was measured from 10–400 Hz with the resolution of 1 Hz. The limit of 400 Hz was chosen because in industrial application, for example, automotive panels are treated with specific measures for the high frequency range. Therefore, the vibrations and acoustic noise can be effectively damped or isolated above 400 Hz. The lower frequency range is liable to vibrations of the structure. Damping systems against mechanical vibrations are required. With the resolution of 1 Hz, the system behavior can already be quite precisely detected together with the curve-fitting tool (see Section 4.1).

As mentioned in Section 2, the behavior of a whole plate should be assessed by many measurement points on the plate. A 5×5 point-grid was chosen as the measuring points. These points are indicated as white spots in Figure 5. The grid locates in the middle area of the plate, where over 60% of the accumulated vibration amplitudes are concentrated. The horizontal and vertical intervals between each two measuring points are 50 and 40 mm respectively. For each mode, notable displacements can be measured from the majority of these points. The measured 25 receptance FRF (laser/impedance head) from 10–400 Hz were converted to a single FRF of RMS receptance. This receptance FRF was further converted to a mobility FRF with the curve-fitting tool for the final evaluation of each sample.

4. Results and discussions

4.1. Resolution test

In order to evaluate the precise behavior of the system, the plates should be tested with possibly exquisite resolutions for the frequency scanning, i.e., with the scanning interval of each 0.1 Hz, the acquired vibration curve is closer to the reality than with 1 Hz interval, for instance. In this situation, the required time for each measurement will be greatly prolonged. It is important to find an optimum resolution with which the behavior of the system can still be recorded without significant deviation to the original vibration but with a reasonable effort for the measuring time. For this purpose, the study of scanning resolution was investigated with several significant peaks of some specimens.

The sample with a simple 4 mm particle damper (see Section 4.4), which has a poor damping efficiency, was mainly investigated. The mode 1, 2, 4, 9 and 10, which have quite high velocity magnitudes were measured to investigate the influence of the resolution under different frequencies. Some peaks from the samples with particle dampers of better performance were also measured to survey the difference between poor and well damped structures. The study is divided into two steps. The resolution limit, which is good enough to represent the reality, will be determined in the first step. Then the differences from coarse to fine resolutions is investigated in the second step.

In the first step, two samples with poor and excellent damping were measured as in Figure 7 with five different resolutions: 1, 0.5, 0.25, 0.1 and 0.05 Hz. From the results it can be observed that the curves of 1 and 0.5 Hz have some difference to 0.25, 0.1 and 0.05 Hz. The distortion is smaller with higher resolutions. The curves of 0.1 and 0.05 Hz overlap well with each

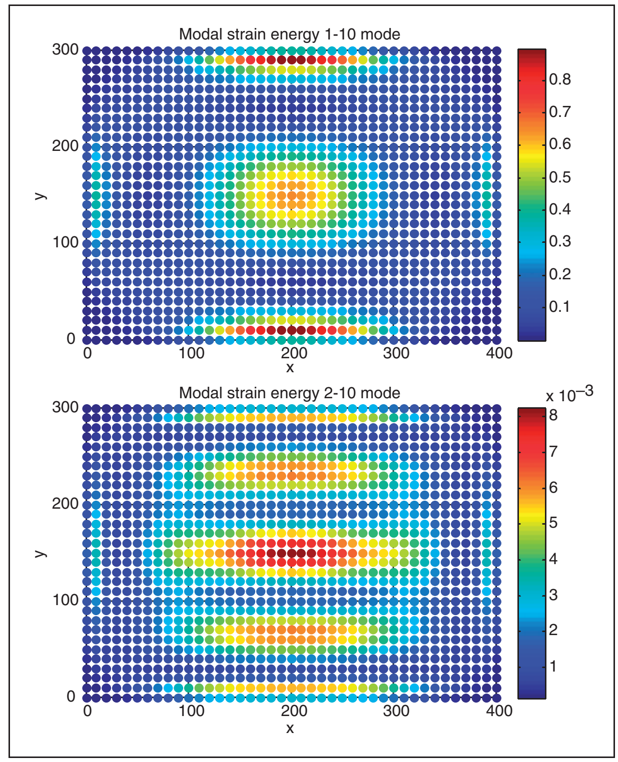

Figure 6. Overlapped modal strain energy.

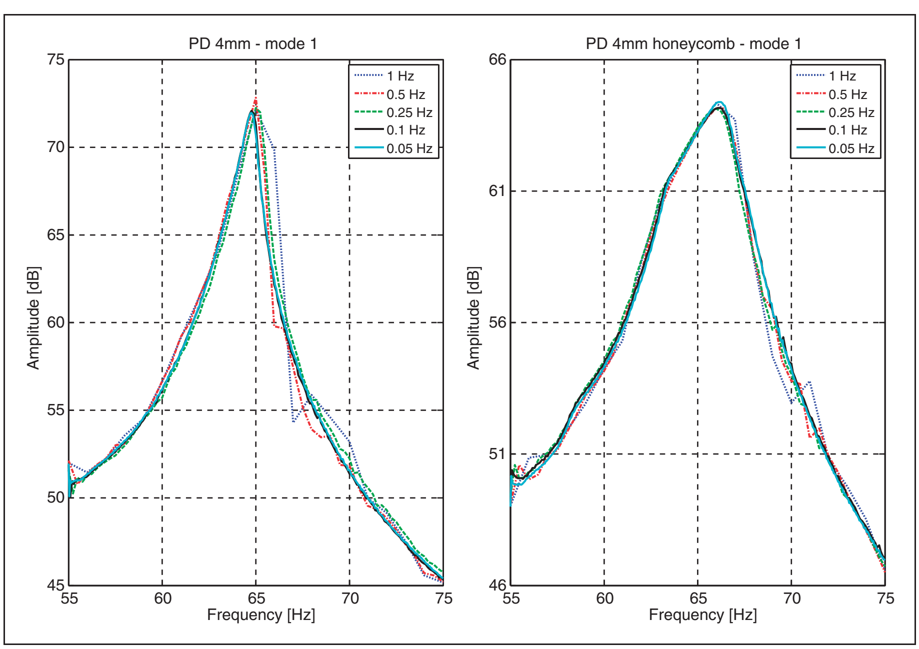

Figure 7. Resonance peaks measured with different resolutions.

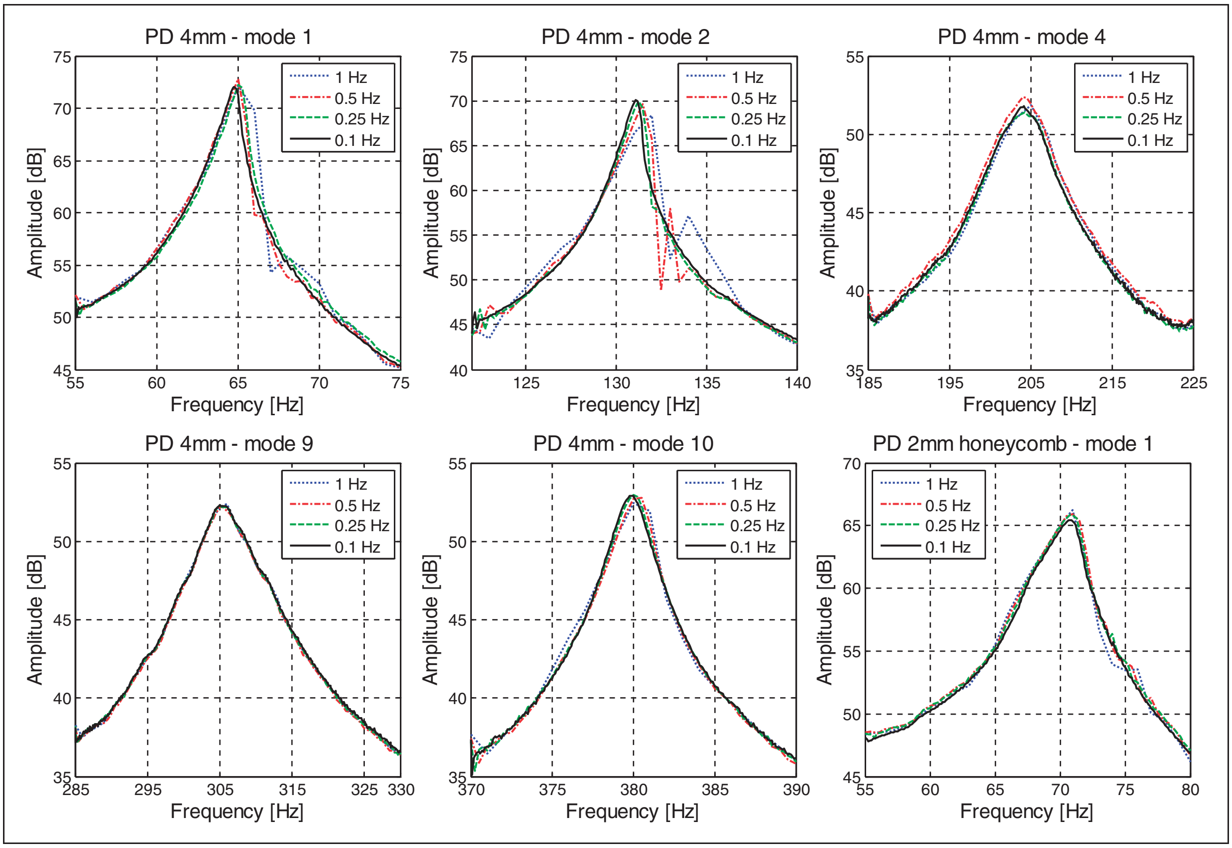

Figure 8. Measured peaks in the resolution study.

other, which indicates that 0.1 Hz is good enough for the measurement. For this reason, the following study was measured only with the first four resolutions until 0.1 Hz.

In the next step, different modes of the sample with 4 mm simple particle damper were measured with these resolutions. From Figure 8, similar tendencies can be observed with the improvement of the resolutions, as in Figure 7. Because these curves don't obey the FRF of an SDOF system, they were fitted with the introduced curve-fitting tool. The final data evaluated with this tool, including resonance frequencies, peak value at the resonance and loss factors are listed in Table 2. From the results it can be seen that the difference of the measured resonance frequencies and peak amplitudes are generally less than 3%. Only the difference between the loss factors can be over 10%. Modes 1 and 2 have the greatest relative differences (15% and 23%). However, the absolute difference is very slight (0.3 [10^{-2}]). For an undamped structure, this difference is insignificant. With the increase of the frequency, the differences get smaller and the signals are more stable, because for similar loss factors, the 3-dB span is wider in higher frequencies. At modes 4 and 9, the differences are reduced to 7% and 2% respectively. Next, the difference between a poor and well damped structure was compared through mode 1 of the 4 mm simple particle damper and the 2 mm honeycomb particle damper, which has an excellent damping efficiency. In the latter, the difference of the loss factor is only 7% (with absolute difference of 0.4 [10^{-2}]). Therefore, the different resolutions have much less influence on a better damped structure than a poorly damped one. It can be concluded that various structures with different damping efficiencies have similar difference of fitted loss factors between the resolutions from 0.1 to 1 Hz. The absolute deviation of 0.3-0.4 [10^{-2}] is tolerable for the evaluation of damped structures. In general terms, for measuring the plates in this contribution, the differences using different scanning resolutions are not critical to the use of the curve-fitting tool. Hence, all samples were measured with 1 Hz.

On the other hand, the plot of mode 2 in Figure 8 shows that the shape of the peak with low damping and coarse resolution is sometimes distorted. With the use of the fitting-tool, it is not only the loss factor that can be assessed in a precise way, but also the distorted curve can be rectified into the right shape. The evaluated loss factor finally reflects the realistic system behavior without distortion. The value with 1 Hz is close to the value of 0.1 Hz.

Table 2. Results of the resolution study

Peak	Fitted parameter	resolution 1 Hz	0.5 Hz	0.2 5Hz	0.1 Hz	Max. deviation	Deviation [%]
PD 4 mm mode 1	f_{res} [Hz]	64.64	64.34	64.61	64.36	0.30	0.5%
	Amp_{res} [dB]	73.4	71.9	71.6	71.4	2.1	2.8%
	η [10^{-2}]	1.73	1.92	2.02	2.04	0.31	15.4%
PD 4 mm mode 2	f_{res} [Hz]	131.23	131.00	130.93	130.84	0.38	0.3%
	Amp_{res} [dB]	68.5	69.2	69.8	69.8	1.3	1.9%
	η [10^{-2}]	0.88	0.74	0.68	0.69	0.20	22.9%
PD 4 mm mode 4	f_{res} [Hz]	204.40	203.99	203.97	203.97	0.43	0.2%
	Amp_{res} [dB]	51.7	52.2	51.4	51.6	0.8	1.5%
	η [10^{-2}]	3.49	3.41	3.65	3.39	0.26	7.0%
PD 4 mm mode 9	f_{res} [Hz]	305.85	305.87	305.83	305.86	0.04	0.0%
	Amp_{res} [dB]	52.1	51.9	52.0	52.1	0.2	0.4%
	η [10^{-2}]	2.61	2.66	2.66	2.65	0.04	1.7%
PD 4 mm mode 10	f_{res} [Hz]	380.02	380.04	379.92	379.86	0.18	0.1%
	Amp_{res} [dB]	52.9	52.9	52.9	52.9	0.1	0.1%
	η [10^{-2}]	0.65	0.63	0.64	0.65	0.02	3.3%
PD 2 mm Honeycom bmode 1	f_{res} [Hz]	70.03	70.21	70.19	70.18	0.18	0.3%
	Amp_{res} [dB]	65.8	65.7	65.6	65.2	0.7	1.0%
	η [10^{-2}]	4.46	4.71	4.73	4.81	0.35	7.3%

4.2. Interface damping (ID)

4.2.1. ID configuration. One butyl rubber was used for the interface damper. The material is modeled with the second order fractional model (Jones, 2001). The complex modulus E^* of the butyl rubber can be expressed by the equations:

$$\mathrm{E}^* = \frac{1.595 + 0.2154 \cdot (\mathrm{i}\omega\alpha(\mathrm{T}))^{0.7753} + 4.19 \cdot 10^{-4} \cdot (\mathrm{i}\omega\alpha(\mathrm{T}))^{1.551}}{1 + 8.877 \cdot 10^{-3} \cdot (\mathrm{i}\omega\alpha(\mathrm{T}))^{0.7753} + 10^{-6} \cdot (\mathrm{i}\omega\alpha(\mathrm{T}))^{1.551}} \tag{7}$$

$$\log_{10}[\alpha(\mathrm{T})] = 4.2914 \cdot 10^3 \left(\frac{1}{\mathrm{T}} - \frac{1}{293.15}\right) \tag{8}$$

Where ω is the angular frequency and T is the temperature in Kelvin. Since all the specimens were measured under room temperature at 24°C, the material Young's modulus and loss factor at this temperature were deduced in Figure 9.

Limited by the production process, the VEM was only available in the thickness of 1.4–1.5 mm. In the experiment two samples were tested to investigate the effect of interface thickness. One was bonded with one layer butyl, and the other was bonded with two layers, which are overlapped in the thickness direction. The overlapped width of the VEM between the plate and the frame is 20 mm on each side and the outer dimension of the overlapped interface is the same as the plate (440 × 340 mm).

The applied butyl rubber was optimized for automotive application and has very good adhesion properties. In order to avoid any unknown effects caused by gluing, the surfaces of the frame and the plate were roughed by sandpaper and then directly bonded together by the butyl rubber without additional adhesive.

4.2.2. ID results. Since the plate and frame are much stiffer than the VEM at the interface, with the vibration from the frame, remarkable deformation at the flexible interface is induced in the VEM, which causes damping. In addition, the stiffness distinction between the components also incurs the decoupling between plate and frame. From the FRF in Figure 10 it can be observed that the resonance peak at each mode of the sample with single layer ID is markedly reduced with 10–20 dB compared to the undamped configuration. By applying two layers of VEM, the vibration attenuation is even stronger. The loss factors of ID are listed in Table 3. On the sample with single layer VEM, all modes are stably damped. The difference between the loss factors at different frequencies is not remarkable. The values between 2.2-3 [10^{-2}] reveal that the amplitude reduction comes not only from the mass effect, but also from the damping

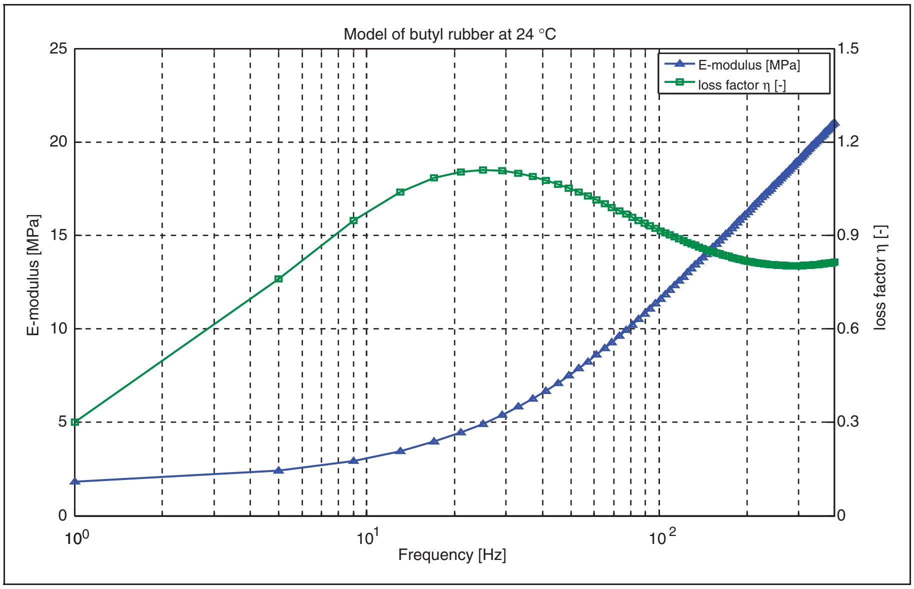

Figure 9. Butyl rubber for interface damping at 24°C.

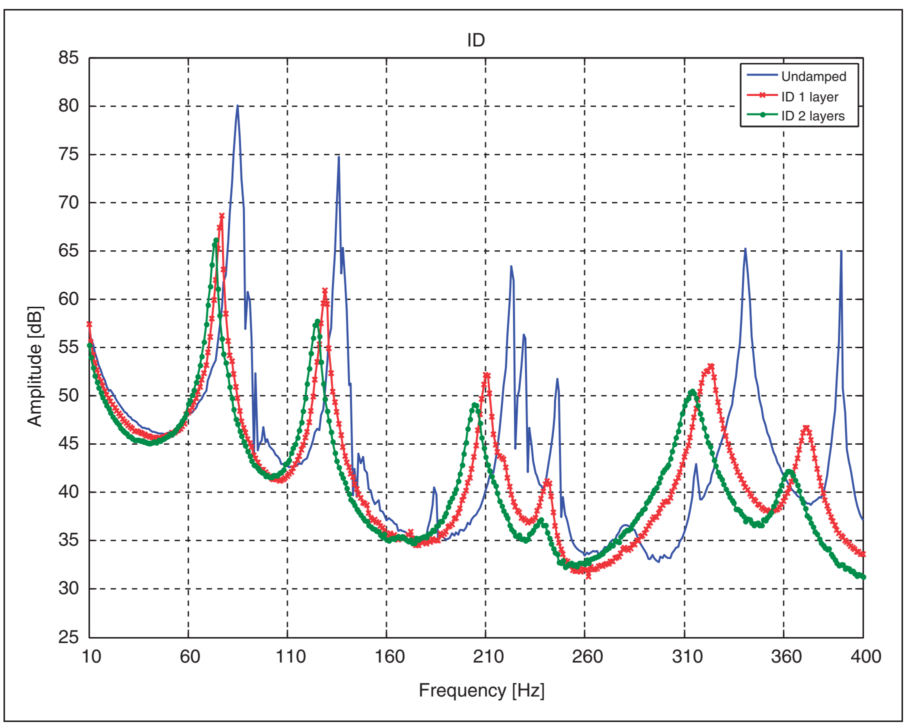

Figure 10. Complete frequency response function of interface damping.

contribution. The characteristic of the ID is that the damping is globally effective for every mode through the whole frequency range of interest. With regard to this aspect, it is superb in contrast to sectional treatments that damp only some modes or areas partially.

Another notable point is that at the global mode (mode 6 at about 240 Hz in Figure 10 and Table 3), ID has the highest loss factor among all the modes. The loss factor reaches 3.05 and 6.42 [10^{-2}] with one or two VEM layers respectively. The intense vibration on the frame at this mode enhances the deformation in the VEM. Thus the plate is strongly decoupled from the vibration on the frame due to the stiffness distinction. In real automotive applications, many global modes of car bodies typically appear below 150 Hz. In these frequencies, the normal surface damping

Table 3. Results of ID for all modes

Specimen/η [10^{-2}]	Mode 1	Mode 2	Mode 4	Mode 6	Mode 8/9	Mode 10
undamped	0.73	0.89	0.48	0.84	0.65	0.13
ID 1 layer	2.96	2.44	2.27	3.05	2.69	2.42
ID 2 layers	3.89	3.70	3.49	6.42	3.40	3.70

Table 4. Properties of piezoelectric elements

Operating voltage	- 50 ~ 200 V
Holding force	90 N
Electrical capacitance	150 nF
Size	61 mm× 35 mm × 0.4 mm

Table 5. ACLD specimens

No.	Specimen	Total gain [-]
1	(A)CLD	without active control
2	ACLD 40	40
3	ACLD 120	120
4	ACLD 240	240

ACLD: active constrained layer damping.

system doesn't work for the panel structures because the deformation within the single panels is usually small. The panel swings with the frame structure in a rigid-like behavior. With ID this type of global modes could be damped.

Briefly, the ID has following features:

- The decoupling and damping effect exist concurrently in ID
- ID is an approach which damps every mode in the investigated frequency range. The performance of ID is very stable at any frequency.
- The decoupling effect isolates the plate well to the excitation source. Soft VEM is better for the isolation.
- ID is the only approach investigated that helps to damp global vibrations from the peripheral structures. Therefore, it is an approach with profound potential for damping automotive panels.

4.3. Active constrained layer damping (ACLD)

4.3.1. ACLD configuration. The ACLD system consists of the damping material (VEM), sensor, actuator and the amplification loop for the actuator. The VEM used in ACLD is the same as that used for ID. As sensor and actuator, two identical DuraAct™ patches were used. The properties of the used piezoelectric sensor and actuator are shown in Table 4.

The amplification loop of ACLD is composed of two steps as shown in Figure 2 – the first step is adjustable for the voltage gain, whereas the second step is an amplifier with fixed gain. For both steps, the proportional amplification of displacement was used as control law. The first step is a non-inverting op-amp. With different excitation amplitudes, the induced voltages on the sensor are different. By adjusting the gain of the first step, the voltages fed to the actuator can be adapted, so that the voltages imposed on the actuator can be controlled in a designed range. Moreover, with the adjustable gain, the influence of different input voltages to the damping performance was investigated. Three gain levels were applied: 2, 6 and 12. The second amplification step is ACX 1224 with a fixed gain of 20 and a voltage output limit of 200 V. These two amplifiers are connected serially. The total gain of the voltage signal is the product of these two separate gains.

The applied specimens of ACLD are listed in Table 5. The first specimen (A)CLD uses exactly the same configuration as the other ACLD samples, except that it was measured without any active control (open loop). The piezo actuator in this case works merely as a passive constraining layer. The other three specimens employ minimal, middle and maximum gain for the voltage amplification (closed loop).

The plate was bonded to the frame by a thin epoxy layer, and the piezo sensor patch was bonded to the plate by epoxy. The actuator, VEM and sensor were bonded with each other merely by the butyl rubber without any adhesives such as those mentioned in the section on ID.

4.3.2. ACLD results. ACLD is an improved variant of CLD. The dimensions of the piezo patches are normally identical to the VEM. i.e., its configuration and characteristics are similar to CLD. Only the efficiency is raised in contrast to CLD due to the active actuating of the VEM. The responses of the ACLD specimens are indicated in Figure 11.

Firstly, we observe the vibration behaviors of the specimens under non-resonant frequencies. In the low frequency range (10–150 Hz), all FRF curves of No.1–4 overlap with each other. The open/close loop control doesn't have any influence on their vibration behavior.

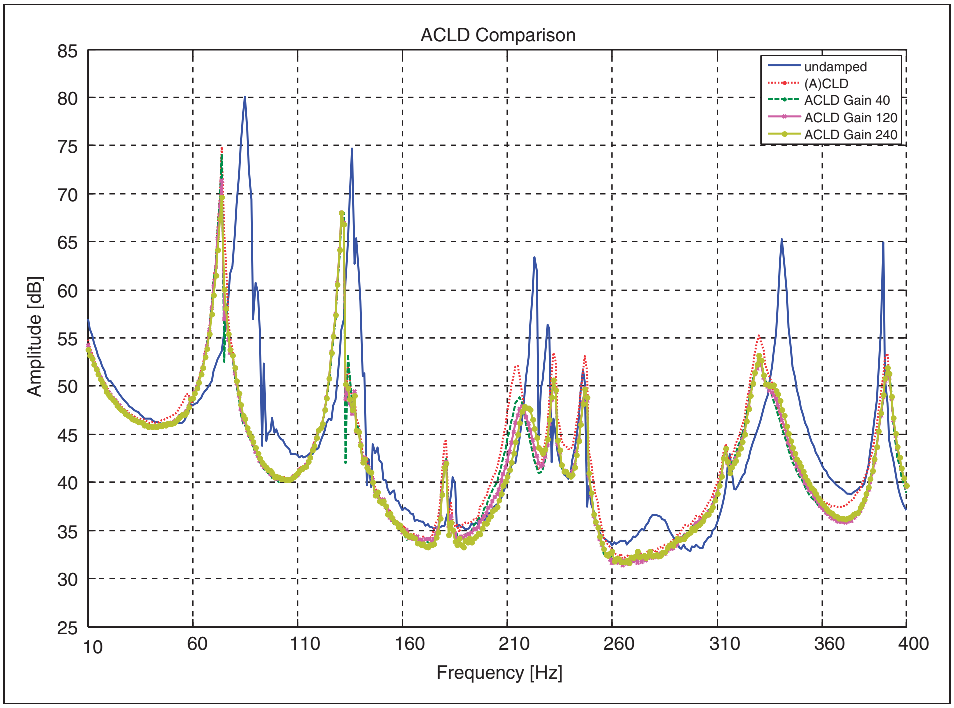

Figure 11. Complete frequency response function of active constrained layer damping.

It reveals that at low frequencies, where the modal wave length of the structure is considerably longer than the length of the CLD segment, no constraining effect is exerted on the VEM layer and the CLD/ACLD treatment doesn't work. Systematic analysis and experimental results on this effect can also be found (Kerwin, 1959; Plunkett and Lee, 1970; Illaire and Kropp, 2004). At 150 Hz, the wave lengths of the structure get shorter. The ACLD becomes more effective. The vibration amplitudes of the passive (A)CLD specimens are globally higher than the close-loop controlled ACLD in the investigated frequency range. Due to the limited frequency range in our test, the wave lengths of the structure are still longer than the size of the piezo actuator. In addition, the sensor and the actuator were located at the nodal position for many of the modes. Consequently, the instability of ACLD due to the spillover effect (Chantalakhana and Stanway, 2001) could not be observed from the results and the close-loop ACLD performs better overall than open-loop (A)CLD.

Next, the responses of resonant frequencies will be observed. The FRF of the damped modes (1, 4 and 9) are shown in Figure 12. On the ACLD 240 sample, the amplitudes are reduced by 5.2 dB (mode 1), 4.2 dB (mode 4) and 2 dB (mode 9) in comparison to the (A)CLD sample, respectively. Although the amplitudes are mitigated, the damping efficiency of ACLD remains moderate for the surveyed samples. At mode 1, the loss factor increases slightly with the amplified voltage in spite of the perceivable amplitude mitigation. The improvement of the loss factor with increasing amplification at mode 4 is pronounced. At mode 9, the differences are not marked. In order to understand these effects, the mode shapes and the position of the actuators at these modes are shown in Figure 13.

At mode 1, the dimension of the ACLD damper is too small to induce sufficient constraining effect in the VEM. Also the strain energy at the middle is moderate compared to the region of the edge, which leads to the inefficiency at this mode. At mode 4, the piezo locates between two consecutive nodes. The half wavelength between these two nodes is close to the piezo patch's longitudinal dimension. The piezo sensor is strongly bent and has a great voltage output. The wavelength is in the adequate range for the damping, which results in the high loss factor at this mode. The deflection of the plate at mode 9 is in the same order as mode 4. However, the piezo sensor experiences a small curvature at this mode, because the wave form is perpendicular to that of mode 4 and therefore is not optimal to actuate ACLD damping elements. The minor deflections of the sensor and VEM cause the resultant low damping. It can be seen that in the damped modes, only some of them can be effectively damped with one ACLD configuration.

The responses at the undamped and global modes are shown in Figure 14. At mode 2, due to the low frequency, all curves overlap with each other. Above mode 2, all other modes including the global mode have almost the same behavior. The curves of the

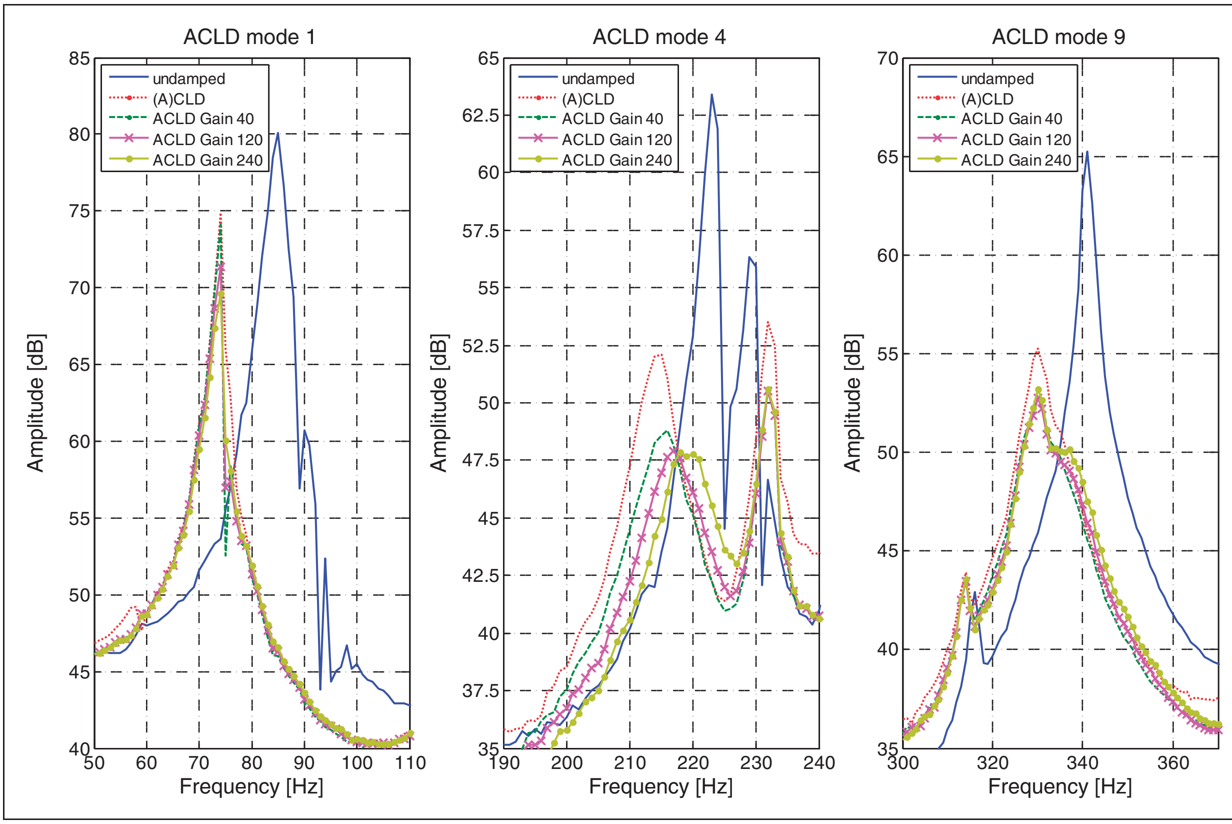

Figure 12. Frequency response function of damped modes (1, 4 and 9) with active constrained layer damping.

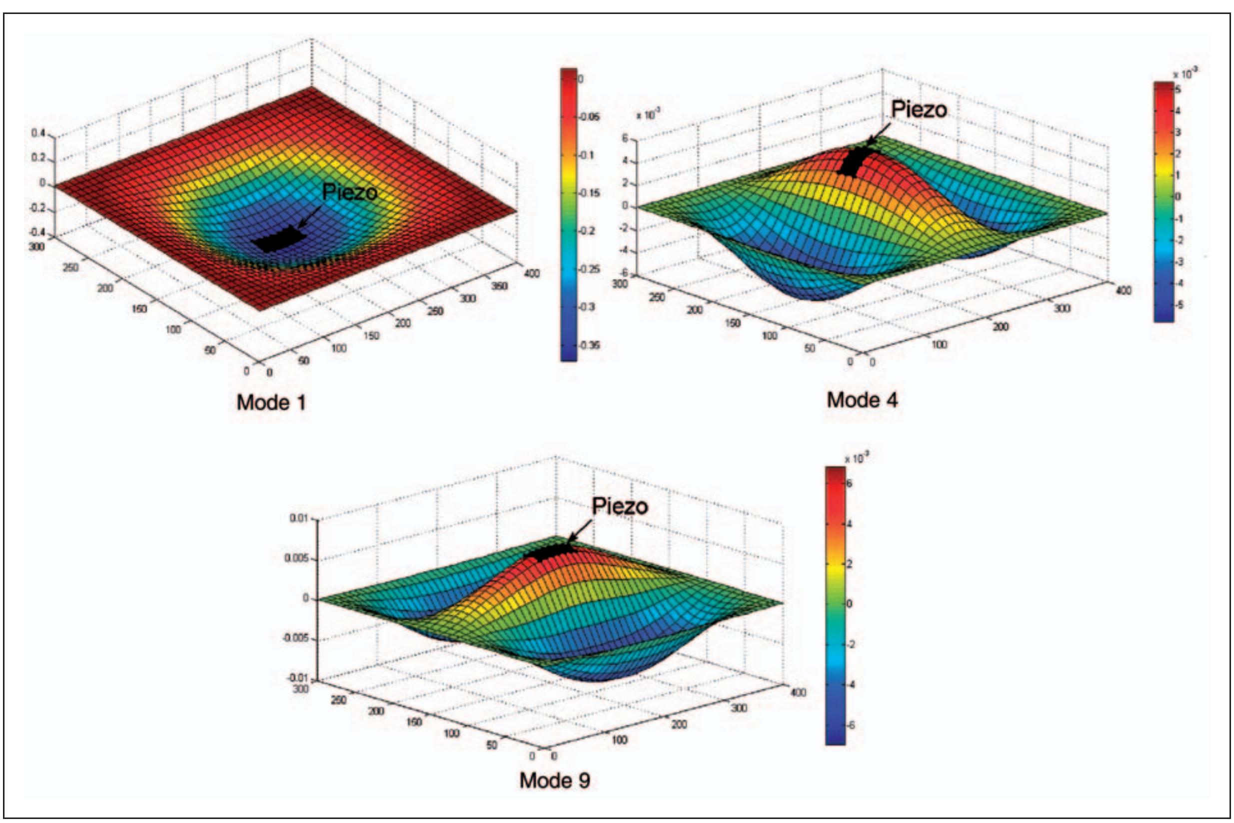

Figure 13. Strain ratio of the piezo elements for modes 1, 4 and 9.

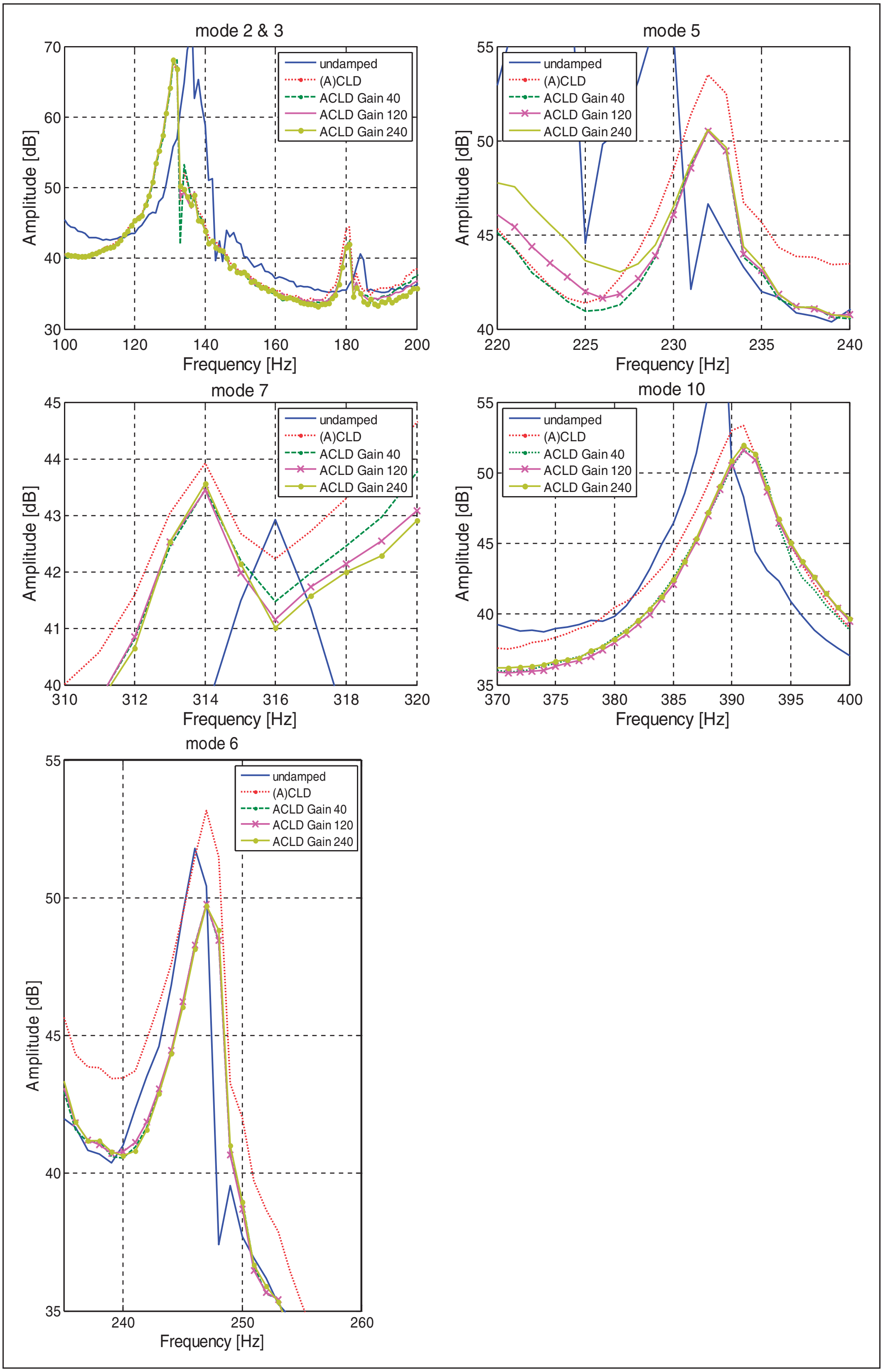

Figure 14. Frequency response function of undamped and global modes with active constrained layer damping.

Table 6. Results of ACLD at damped modes

Damper	Mode 1		Mode4		Mode 8/9	
	Amp.[dB]	$\eta[10^{-2}]$	Amp.[dB]	$\eta[10^{-2}]$	Amp.[dB]	$\eta[10^{-2}]$
(A)CLD	74.9	1.71	52.1	2.76	55.2	1.94
ACLD gain 40	74.1	1.65	48.8	3.62	53.1	1.47
ACLD gain 120	71.4	2.05	47.9	4.08	52.7	1.51
ACLD gain 240	69.6	2.50	47.9	4.27	53.2	1.77

ACLD: active constrained layer damping

Table 7. Loss factors of ACLD at undamped and global modes

Specimen/$\eta[10^{-2}]$	Mode 2	Mode 3	Mode 5	Mode 6	Mode 7	Mode 10
undamped	0.89	1.66	0.85	0.84	1.16	0.13
(A)CLD	1.46	1.06	0.99	0.99	1.20	1.02
ACLD gain 40	1.45	1.01	1.05	1.04	1.17	1.08
ACLD gain 120	1.52	1.00	1.07	1.05	1.12	1.14
ACLD gain 240	1.48	0.95	1.12	1.07	1.11	1.11

ACLD: active constrained layer damping

ACLD overlap at the resonances. The amplitudes of the passive (A)CLD are higher than the ACLD. Except for the difference between (A)CLD and ACLD, no improvements can be seen by enhancing the active voltage. The calculated loss factors are listed in Table 7. There is no significant difference between the undamped and the ACLD specimens. As expected, ACLD as a sectional damper doesn't contribute noticeably to the damping of the undamped and global modes.

The characteristics of ACLD can be deduced from the aforementioned effects:

- ACLD is generally ineffective in a low frequency range, where the structure modal wavelength is bigger by far than the sensor dimension. At resonances the improvement through close-loop is limited, while at non-resonant frequencies no difference can be determined. However, the efficiency should be higher than measured in this paper since the position of ACLD elements was suboptimal at mode 1.
- In a high frequency range with short modal wavelengths of the structure, ACLD shows a globally better performance. At resonances, significant damping can be observed.
- The performance of ACLD is sensitive to the location. Both high relative strain in the sensor and the adequate structure wavelength in the longitudinal direction of the sensor/actuator are necessary for a good damping efficiency.
- The bending stiffness of the panel should be higher than the piezo element so that the sensor undertakes sufficient strain.
- For the optimization of CLD or ACLD, sophisticated consideration should be given to different passive and active parameters. For example, the shear parameter g* (Jones, 2001)
- ACLD should be designed for addressing the damping of some specific modes. As in our test case, few damped modes can be mitigated, while undamped and global modes are barely influenced by the damper.

4.4. Particle damping (PD)

4.4.1. PD configuration. In order to survey the parameters of particle damping, six different particle dampers were manufactured, as listed in Table 8. The cross-section areas of the dampers are 60 mm in length and 30 mm in width. Only the depths are varied. In three of them, additional honeycomb cells with the cell size of 3.2 mm were bonded inside the damper container (see Figure 15). The applied particles are between ca. 0.3 and 0.9 mm.

The purpose of using honeycomb cells in the container is to investigate the influence of container size to the damping efficiency between the dampers with and without any interim cell walls. The augmentation of the damping with doubled quantity of particles can be compared with the 2 mm and 4 mm thick samples (No.1 vs. No.5, No.3 vs. No.6). By separating a 4 mm damper into 2×2 mm with a cover in the depth direction (No.2 vs. No.5, No.4 vs. No.6), the relationship of energy dissipation between the particles and between particles and cover wall can be determined. There were three further damper substitutes tested which

Table 8. Particle damper configurations

No.	Type	Damper depth	Total damper weight [g]	Weight of particle [g]
1	Simple	2 mm	25.9	8.3
2	Simple	2×2 mm	45.2	15.6
3	Honeycomb	2 mm	24.7	6.8
4	Honeycomb	2×2 mm	44.7	14.0
5	Simple	4 mm	40.9	16.2
6	Honeycomb	4 mm	39.1	13.2
(7)	Honeycomb substitute	2 mm	24.6	0
(8)	Honeycomb substitute	2×2 mm	44.6	0
(9)	Honeycomb substitute	4 mm	38.9	0

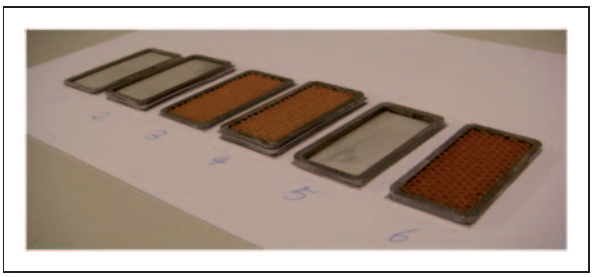

Figure 15. Particle damper containers.

have the same weight as the honeycomb dampers but don't contain any particles. With these substitutes, the performance of the particle dampers can be compared with the undamped structure transversely under the same weight and stiffness condition.

The plate was bonded to the frame by a thin epoxy layer. Because there are a lot of PD configurations, in order to minimize the internal damping difference of different specimens, the different PDs were flexibly bonded to the same specimen. On the contact surface between PD and plate, a thin double-sided tape was applied. On the contrary side of PD, it was firmly fixed to the plate surface with a thin polyimide foil. After each measurement, the PD was removed and replaced by a new one to be measured.

4.4.2. PD results. The responses of the PD at damped modes were investigated first. The simple PD were not efficient (see Figure 16) in the experiments. Their loss factors at the damped modes are less than 2 [10^{-2}] on all samples. These values are only slightly larger than an undamped plate. The difference of damping between samples is not distinct. The low damping is caused by the test setup: the flat particle damper is placed vertically in the experiment. The specimen was excited in the horizontal direction with the shaker. The particles in the bottom layers are compressed by the particles in the upper layers through the gravitation, and the upper part of the damper is hollow. During the horizontal vibration, particles are consolidate more strongly with the increase of the damper length downwards. The force chains generated by the compression between particles provide static instead of sliding frictions, which also hampers the motion of particles and the energy dissipation. Only at the top part in the damper cavity do minor numbers of particles vibrate freely. Due to the tremendous diminishing of the effective particles, the simple PD is in fact added as nothing other than a weight slug with slight damping effects. Thus, these simple PD don't perform appropriately in the tested configuration and cannot present the real behavior of PD due to the deficient placement and damper structure design. The deviation of the loss factors can be quite large compared to the slight measured damping, because the exact quantities of the unconstrained particles in each PD stay unknown. For the vibration in a horizontal direction, the big length–depth ratio of the dampers augments the compression effect caused by gravity, which should be avoided.

In contrast with the simple PD with a single container cavity for particles, the influence of the container size was investigated with the honeycomb dampers, in which the same quantity particles are separated in several small sections instead of a single big cavity. With many 3.2 mm honeycomb cells, the damper is divided into more than 100 separate small cavities. In this case, although there are almost same weight of particles in this honeycomb damper as the simple PD, most of the particles in each cell are not tightly compressed by the gravity, due to the moderate amount. By locating in a vertical direction, the particles are still able to move in the small honeycomb cells during the horizontal vibration. All these active particles contribute to significant damping, as can be seen in Table 10. The measured loss factors of the honeycomb PD are 1.8 to 3.9 times higher

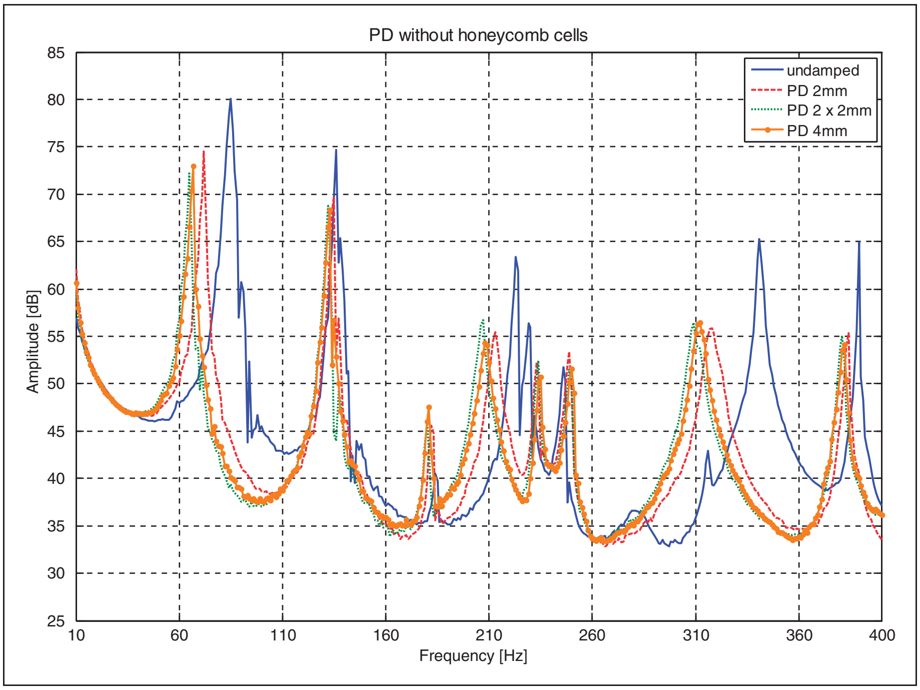

Figure 16. Frequency response function of simple particle damping.

Table 9. Simple PD results at damped modes

	Mode 1		Mode 4		Mode 8/9	
Damper	Amp.[dB]	$\eta[10^{-2}]$	Amp.[dB]	$\eta[10^{-2}]$	Amp.[dB]	$\eta\ [10^{-2}]$
2 mm	74.5	1.47	55.5	1.95	55.9	1.96
2×2 mm	72.2	1.97	56.7	1.89	56.4	1.19
4 mm	72.9	1.68	54.3	2.40	56.4	1.56

PD: particle damping

Table 10. Results of honeycomb PD at damped modes

	Mode 1		Mode 4		Mode 8/9	
Damper	Amp.[dB]	$\eta\ [10^{-2}]$	Amp. [dB]	$\eta\ [10^{-2}]$	Amp. [dB]	$\eta\ [10^{-2}]$
2 mm H	65.8	4.68	51.5	3.26	51.3	3.60
2×2 mm H	64.7	5.48	52.2	3.52	51.9	2.96
4 mm H	63.4	6.58	51.4	3.80	49.8	4.06

PD: particle damping; H: honeycomb

than those simple PD at the damped modes. With doubled weight, the loss factors of the 4 mm honeycomb damper are improved by 11–29% compared to the 2 mm honeycomb damper. Hence, separating cavities in the proper direction is meaningful to avoid the compression caused by gravity.

The influence of the cover wall was determined with the specimens of 2×2 mm honeycomb and 4 mm honeycomb damper (No. 4 and No. 6 in Figure 15). No. 6, with even less weight of particles, performs even better than No. 4. The cover wall reduces the amount of the particles and their chances of collision with each other in a single closed cavity. This results in the degradation of the damper performance. Therefore, with the same amount of particles, the damper with a single cavity in the vibration direction surpasses those

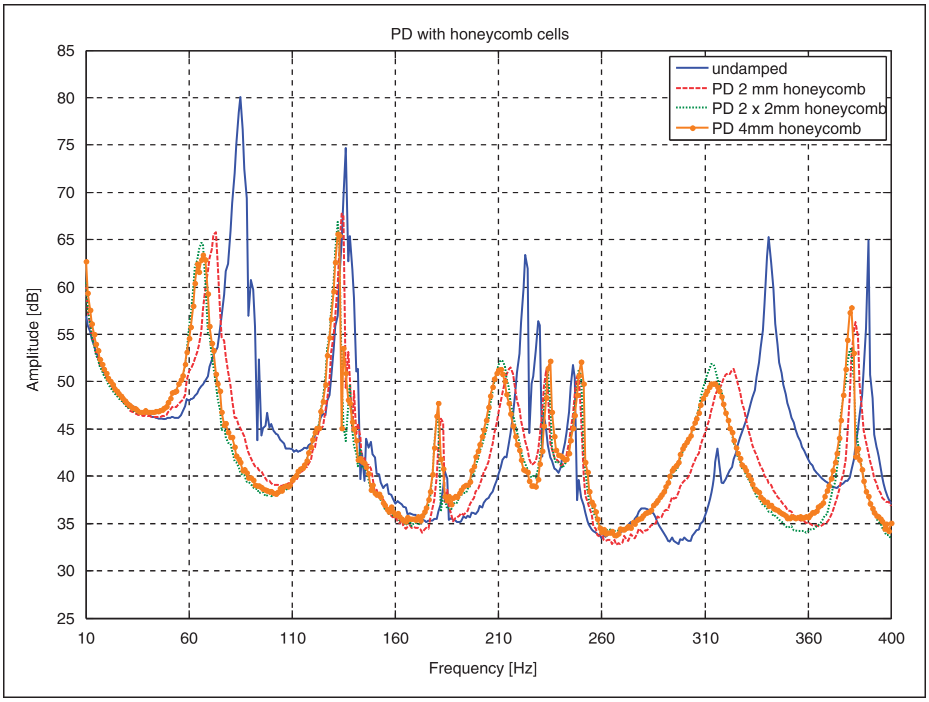

Figure 17. Frequency response function of honeycomb particle damping.

with several cavities, if most particles are not highly constrained for their motions. i.e., separating cavities across the vibration direction is detrimental for the damping performance.

As the honeycomb PD (Nos. 3, 4 and 6) performs superbly, they were further compared with the weight substitute samples No. 7–9, in order to survey the absolute performance of honeycomb PD in contrast with undamped structures. On the substitute samples, one single metal slug with the same weight as the honeycomb damper is bonded at the midpoint of the plate. Because both weight and stiffness of the two type samples are the same, accurate comparisons of the damping can be directly observed in Figure 18 and Table 11.

We still observe the damped modes 1, 4 and 9. The honeycomb PD are generally very effective for suppressing the first mode. A decay of 13–16 dB with the honeycomb PD corresponds to an amplitude attenuation of 78–84%. For modes 4 and 9, the amplitudes of particle damper samples were reduced in the range of 2–5 dB compared with the weight substitute samples. The loss factors were improved by 27–60%.

The loss factors of the undamped and global modes are listed in Table 12. As with the behavior of ACLD at theses modes, the difference of the values is also indistinct with PD. No additional damping can be attained at undamped and global modes.

An insight into the damping efficiency between an undamped sample with simple PD and a honeycomb PD damped sample (4 mm thick weight slug/damper) is given in Figure 19. In each plot, the mean mobility of the accumulated magnitude on the 25 measured points from 10–400 Hz is shown. As also seen in Figure 5, the vibration of an undamped plate (substitute) looks like the dominant 1st mode. The sample with simple PD has similar behavior. But the amplitude at the midpoint is slightly mitigated and the magnitudes at each point are globally lower than the undamped sample. The concave surface of the honeycomb damper sample shows tremendous amplitude attenuation at the midpoint. Even the points at its vicinity are accompanied damped. The vibrations at each point are further damped in contrast to simple PD.

Concisely, the characteristics of PD can be concluded as below:

- The appropriate applied PD has superior damping capability with relatively good stability (insensitive to temperature or frequency)
- The behavior of PD is dependent on the vibration direction
- The optimal shape and placement of the PD is highly dependent on the real vibration situation (mainly direction)
- The vibration direction is the effective direction of PD. PD should possibly possess less cavities in this

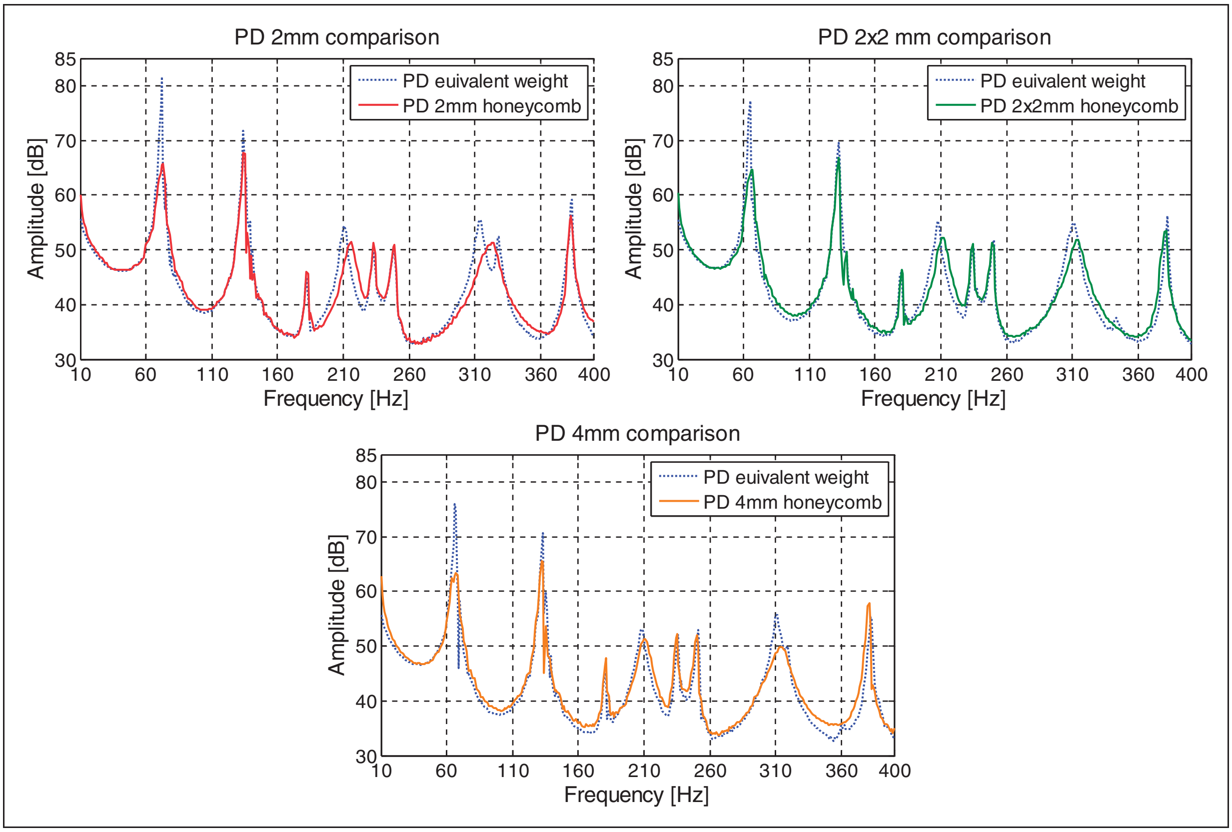

Figure 18. Frequency response function of the honeycomb particle damping vs. undamped sample with same weight.

Table 11. Results of honeycomb PD with equivalent weight samples at damped modes

	Mode 1		Mode 4		Mode 8/9	
Damper	Amp.[dB]	η [10^{-2}]	Amp.[dB]	η [10^{-2}]	Amp. [dB]	η [10^{-2}]
2 mm weight	81.7	0.01	54.4	2.13	55.5	1.74
2 mm honeycomb	65.8	4.68	51.5	3.26	51.3	3.60
2×2 mm weight	77.2	0.44	55.3	2.12	55.0	2.08
2×2 mm honeycomb	64.7	5.48	52.2	3.52	51.9	2.96
4 mm weight	75.9	0.94	53.2	2.77	55.7	1.61
4 mm honeycomb	63.4	6.58	51.4	3.80	49.8	4.06

Table 12. Results of honeycomb PD at undamped and global modes

Specimen/η [10^{-2}]	Mode 2	Mode 3	Mode 5	Mode 6	Mode 10
Undamped	0.89	1.66	0.85	0.89	0.13
2 mm honeycomb	0.81	1.15	1.08	1.04	0.53
2×2 mm honeycomb	0.99	1.16	0.99	1.05	0.73
4 mm honeycomb	1.19	1.25	0.93	1.08	0.45

PD: particle damping

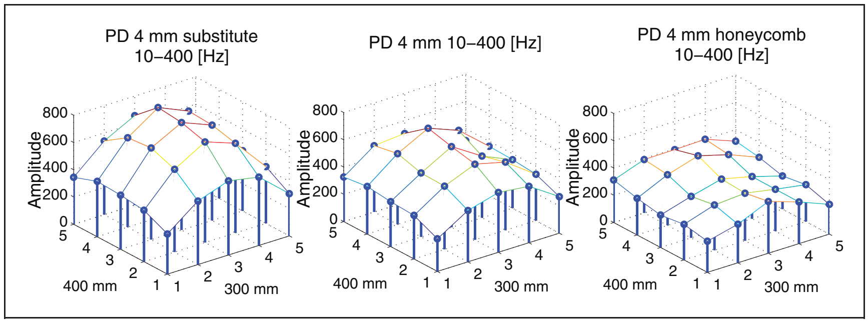

Figure 19. Vibration shapes of the 4 mm particle damping specimens.

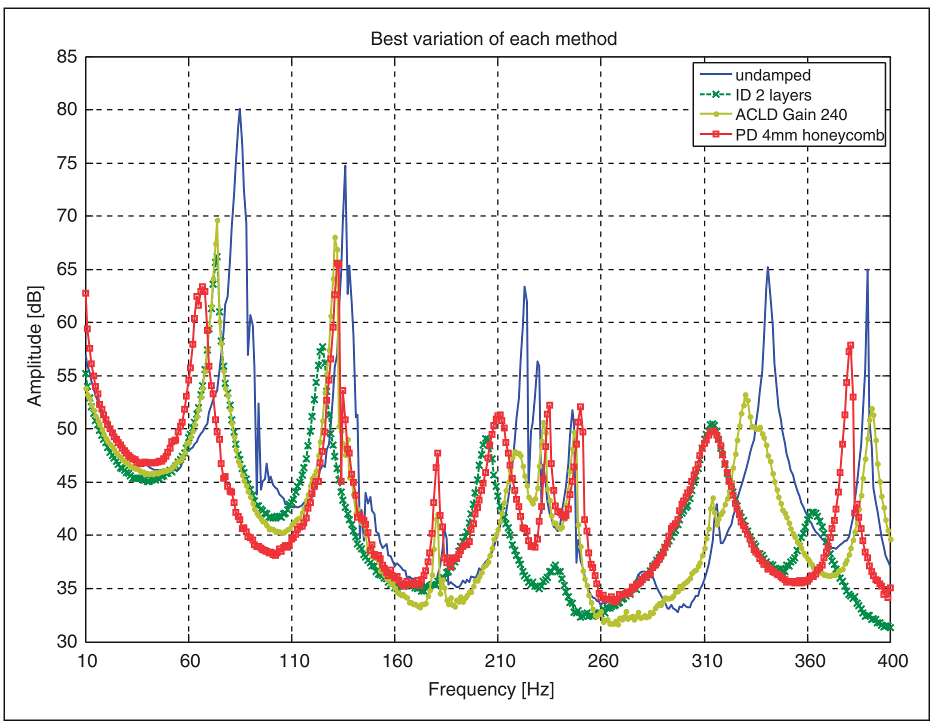

Figure 20. Specimens with best performance of each approach.

direction and more particles should be filled into one cavity in order to raise the efficiency. A big depth–length ratio of the cavity is advantageous.

- Meanwhile the effect of compression of the consolidated particles should be avoided. A cavity with a filling ratio of 90–95% is optimal (Liu et al., 2010).
- The cavities should be vertically kept with proper size to avoid gravity compression in the case of horizontal excitation
- Cellular insert is a solution to solve the ''anisotropic'' damping behavior of PD
- At damped modes, PD performs particularly excellently for the first mode. Modes of higher order can still be well damped. PD should be applied at the position with great displacement/velocity
- At undamped and global modes, the damping of PD is negligible
- Structural-borne noise can be effectively damped by PD

5. Conclusion

In this section the performance of the different damping approaches and specimens are compared with their magnitude of the FRF responses, loss factors and weight specific damping efficiencies, transversely considering the frequency influence. Their primary features, advantages and drawbacks are concluded.

The magnitude FRF of the three best specimens from ID, ACLD and PD are shown in Figure 20 for the whole

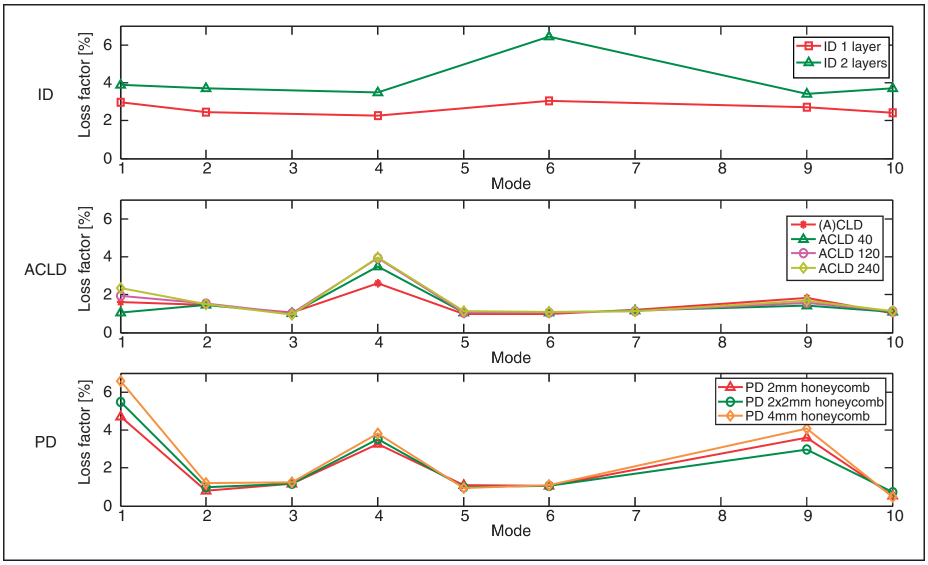

Figure 21. Loss factor of every mode.

frequency range. The FRF of ID show that its average magnitude is the lowest and some modes with small amplitudes are even eliminated. But for a specific mode, its performance can be inferior to PD or ACLD. However, at global mode (frame resonance at 240 Hz), ID mitigates the vibration strongly while ACLD and PD do not significantly affect the vibration behavior. The FRF of PD shows, at mode 1, that the magnitude is superiorly damped by PD compared with ACLD and ID. At mode 9, PD still mitigates the modes better than ACLD. The FRF magnitude of ACLD is quite high below 150 Hz. Nevertheless, it suppresses the vibration more remarkably than PD and ID at mode 4. No approach surpasses the others in terms of amplitude suppression within the whole frequency range.

The modal loss factors of each sample are shown in Figure 21. ID with one layer shows stable performance through the whole frequency range. At global mode, ID has a high loss factor whereas the other two approaches are inefficient for this mode. The effective range of ACLD concentrates on one mode in this study. The other damped modes are not damped or are only slightly damped. At mode 4, a great difference can be seen between open and close-loop. The PD is effective at all frequencies at antinodes. At mode 1, PD provides excellent damping and outperforms ID and ACLD (due to suboptimal damper position) considerably. At mode 4, the loss factors of PD are still high and in the same order as ACLD, while ACLD has already reached its maximum. At mode 9, the loss factors of PD remain high in spite of different mode/wave shape of the structure.

In Figure 22 the mean loss factors of the measured samples are presented in relation to their damper weights. We can see that ACLD has the lowest weight, PD has the intermediate weight, and ID has the highest weight.

The loss factors were calculated for damped, undamped, global and all modes, respectively. The noticeable point is that, sectional dampers (ACLD and PD) perform better only at the damped modes (1, 4 and 9). If the undamped and global modes or whole frequency range is concerned, their efficiencies drop drastically. Conversely, ID still shows similar or even better values. As a consequence, the performance of ID is actually raised compared to the sectional dampers in these cases.

ID exhibits reasonable damping at damped modes. The mean value of one layer lies in the same order as the ACLD and two layers close to PD. Thanks to its stable damping at any frequency, the efficiencies do not change greatly in all the modes. Inversely, for 10 modes, the damping is raised slightly, because ID damps better at global resonance modes. This means that the absolute damping of ID one layer is already competitive with PD. ID of two layers even exceeds any other investigated dampers.

The average efficiencies of ACLD are quite limited. By applying different voltage gains, the loss factor of ACLD can be solely raised by 1.4–2.2 [10^{-2}] above the value of an undamped plate. The difference of loss factors between open and close-loop is about 30% for the damped modes. At undamped and global modes, the loss factors are almost the same as the undamped specimen. Thus, for all modes, the difference between open and close-loop is reduced to about 20% because of the narrow frequency range of effectiveness. Consequently, ACLD has the poorest damping value over the whole frequency range among all investigated treatments.

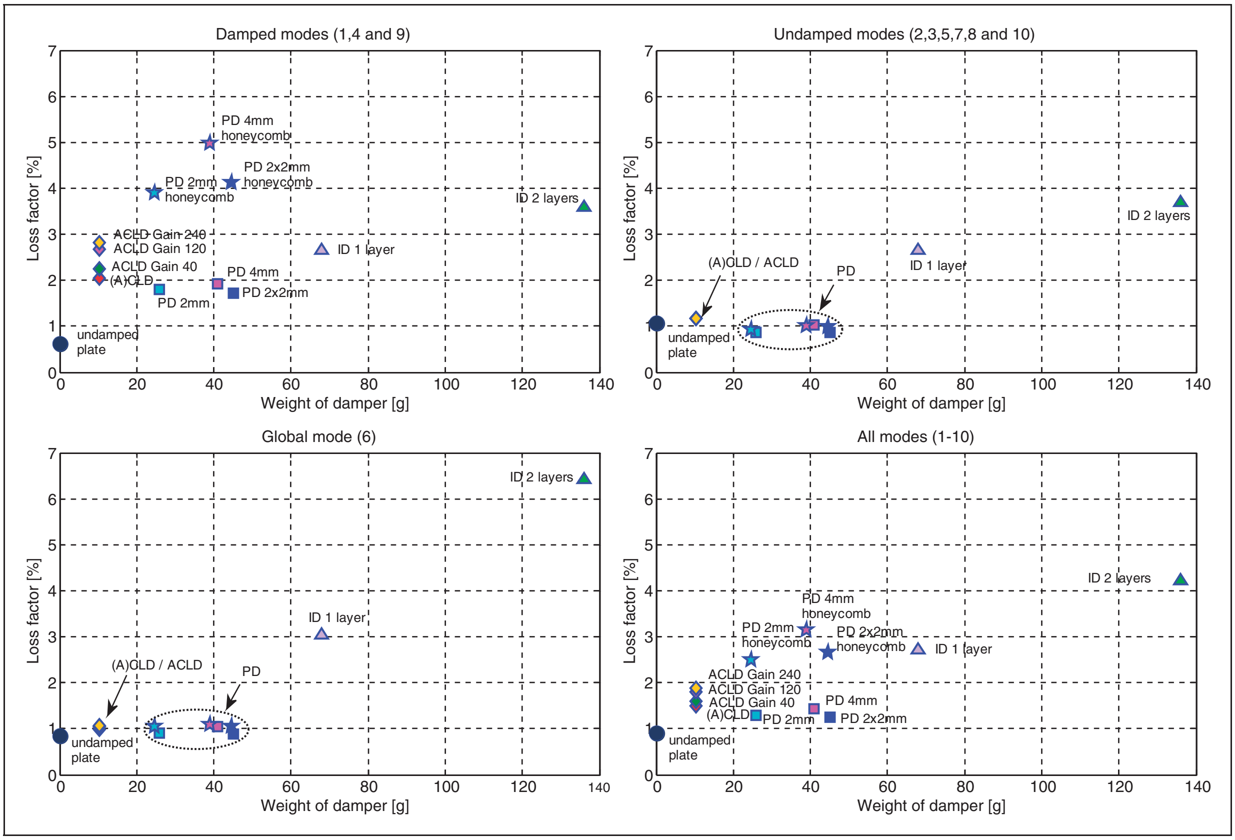

Figure 22. Mean values of specific loss factors in relation to weight.

The PD possess polarized results. Simple PD have very low damping efficiency because of the lack of active movable particles. Thus, these inappropriate configured dampers have much lower damping efficiencies than the other dampers at the damped modes. This shows that the effective use of the particle weight with efficient configuration is an important aspect for PD. The performances of the honeycomb PD are greatly improved in contrast with simple dampers at the damped modes. They have the highest values for both absolute and weight specific loss factors by reaching maximal 5 [10^{-2}]. But like ACLD, the loss factors of PD are negligible at the undamped and global modes. By analyzing all 10 modes, the loss factors reduce drastically by 36–37% due to the poor damping at undamped and global modes. In spite of that, their loss factors are still relatively high and superior to most of the other dampers for the whole frequency range. For both simple and the additional honeycomb PD, the intermediate cover wall in 2×2 mm specimen makes the damping efficiency deteriorate.

With all the phenomena observed above, the characteristics of the three damping approaches can be summarized as the following points:

- The interface damper (ID) acts stably in the whole frequency range. It is especially effective on suppressing the vibrations caused by the resonances from the peripheral environment, which is beneficial for damping automotive panels. ID is suitable for a situation where global damping or isolation of every mode is necessary, while no local mitigation is specially required. The weight of ID is relatively heavy, but with regard to the unavoidable weight of conventional adhesive at the interface, the weight efficiency of ID is still high.
- The active constrained layer damper (ACLD) has a finite frequency range for the application. The lower modes with long wavelengths would require damper elements of a big area. It is effective to damp modes with a patch size similar to the half wavelength of the structure. ACLD is sensitive to the localization and its actuation direction. It is adequate to damp local deflections at a specific frequency (wavelength and direction). Compared with PD, another advantage of ACLD is that its efficiency is independent of the plate orientation. ACLD is a lightweight solution where external power source and control systems are required.

- The particle damper (PD) has superior damping performance. In low frequencies, the efficiency is excellent while in high frequencies high damping can still be obtained. By adjusting the configuration of the particles, container or vibration direction, a great difference of PDs performance can be seen. PD has intermediate weight among the three damping approaches.

These damping approaches behave quite differently with respect to the frequency range, their geometric size and the applied locations. Corresponding to the vibration behavior of the panel structure, e.g. critical frequency range, mode pattern (distribution of critical vibration positions) and other specific requirements, the appropriate damping method for the panel should be selected according to the advantages of these approaches. ID is the unique treatment to effectively damp intense vibrations from the peripheral excitation source. For mitigating any specific local vibration on the structure at finite frequency, ACLD is a good option. If the aim is to have a high damping primary in the low frequency range and concurrently a steady efficiency in a broad frequency range is desired, PD should be applied. Using a combination of global dampers (ID) and sectional dampers (PD, ACLD), it is possible to control all the modes in the frequency range of interest.

Funding

This work was supported by Autoneum AG.

References

ASTM E756 (2005) Standard test method for measuring vibration-damping properties of materials, available from http://www.astm.org/Standards/E756.htm.

Bapat CN and Sankar S (1985) Single unit impact damper in free and forced vibration. *Journal of Sound and Vibration* 99: 85–94.

Chantalakhana C and Stanway R (2001) Active constrained layer damping of clamped-clamped plate vibrations. *Journal of Sound and Vibration* 241: 755–777.

Ewins DJ (2000) *Modal Testing: Theory, Practice and Application*, 2nd edn. Philadelphia, USA, Research Studies Press Ltd.

Hac A and Liu L (1993) Sensor and actuator location in motion control of flexible structures. *Journal of Sound and Vibration* 167: 239–261.

Illaire H and Kropp W (2004) Quantification of damping mechanisms of active constrained layer treatments. *Journal of Sound and Vibration* 281: 189–217.

Johnson CD (1995) Design of passive damping systems. *ASME Special 50th Anniversary Design Issue* 117: 171–176.

Jones DIG (2001) *Handbook of Viscoelastic Vibration Damping*. New York: John Wiley & Sons Ltd.

Kerwin EM (1959) Damping of flexural waves by a constrained viscoelastic layer. *Journal of the Acoustical Society of America* 31: 952–962.

Levenberg K (1944) A method for the solution of certain problems in least squares. *The Quarterly of Applied Mathematics* 2: 164–168.

Liu Y, Sanchez A, Zogg M and Ermanni P (2010) A comparative experimental study on structural and interface damping approaches for vibration suppression purposes. *Proceedings of the SPIE – The International Society for Optical Engineering* 7643: 764335–764345.

Marquardt D (1963) An algorithm for least-squares estimation of nonlinear parameters. *SIAM Journal on Applied Mathematics* 11: 431–441.

Masri SF (1970) General motion of impact dampers. *Journal of the Acoustical Society of America* 47: 229–237.

Panossian HV (1992) Structural damping enhancement via nonobstructive particle damping technique. *ASME Journal of Vibration and Acoustics* 114: 101–105.

Plunkett R and Lee CT (1970) Length optimization for constrained viscoelastic layer damping. *Journal of the Acoustical Society of America* 48: 150–161.

Popplewell N and Semercigil SE (1989) Performance of the bean bag impact damper for a sinusoidal external force. *Journal of Sound and Vibration* 133: 193–223.

Ro J and Baz A (2002) Optimum placement and control of active constrained layer damping using modal strain energy approach. *Journal of Vibration and Control* 8: 861–876.

Stanway R, Rongong JA and Sims ND (2003) Active constrained-layer damping: a state-of-the-art review. In *Proceedings of the Institution of Mechanical Engineers Part I. Journal of Systems and Control Engineering* 217: 437–456.